



Norwegian University of
Science and Technology

Rapid synthesis and structure control of carbon spheres by ultrasound method

Wei Ge

Chemical Engineering

Submission date: June 2016

Supervisor: De Chen, IKP

Norwegian University of Science and Technology
Department of Chemical Engineering

PREFACE

This master thesis has been conducted during the spring semester in 2016 at the Norwegian University of Science and Technology. This project is supported by Statoil. Statoil is one of the largest operators in Norway, and a license holder in abundant oil and gas field.

I feel grateful that I have received plentiful help from my supervisor professor De Chen, and co-supervisor Dr. Qinjun Chen. They have always been inspired and encouraged me during the whole semester.

I would like to thank my supervisor professor De Chen, co-supervisor Dr. Qinjun Chen for academic guidance through the project. In addition, I want to thank Yanyin Qi, Yahao Li, Ting Cui for valuable advises upon my thesis writing. Finally, I would like to thank my family and my friends, Benedicte Hovd, Stine Lervold, Vegard Naustdal, Yalan Wang, Di wang and Mads Lid for their unlimited support.

I declare that this is an independent work according to the exam regulations of the Norwegian university of science and technology (NTNU)

Trondheim, 20 June 2016

Wei Ge



ABSTRACT

The rapid synthesis (within five minutes) of truly monodispersed carbon spheres (CS) using an ultrasonic method was consistently maintained by systematically optimizing various experimental parameters (e.g. catalyst concentration, solvent composition, ultrasonic power, ultrasonic time, reaction temperature, and precursor concentration).

Uniform nitrogen doped carbon spheres (N-CS) are for the first time successfully fabricated by ultrasonic method using resorcinol and formaldehyde as carbon precursors, melamine as nitrogen source. The effect of fabrication parameters on the morphology and structure of the spheres was systematically investigated. The diameters of the N-CS are successfully tuned from nano-scale to submicro-scale (40-1000 nm) by varying the catalyst concentration. In general, the diameter of the N-CS decreases with increasing the concentration of the catalyst. The surface area and pore volume of the N-doped CS before activation were up to $642.0\text{m}^2/\text{g}$ and $0.834\text{m}^3/\text{g}$, respectively. The possibility of activation of N-CS using phosphoric acid (H_3PO_4) was subsequently studied in here.

Modified porous CS was successfully synthesized using resorcinol and formaldehyde as carbon precursor and silica nano-particles as template. Morphology and structure of the Si-template modified CS were also studied in this work.



CONTENTS

Preface	i
Abstract	iii
Contents	v
List of figures	viii
List of tables	x
List of abbreviations	xi
1 Introduction	1
2 Literature review	3
2.1 Development and outlook of monodispersed sphere	3
2.2 Different approaches of carbon sphere synthesis.....	3
2.2.1 Emulsion polymerization	3
2.2.2 Hydrothermal approach	4
2.2.3 Ultrasounds irradiation method.....	5
2.4 Nitrogen doped carbon spheres.....	6
2.5 Application of carbon spheres	7
2.5.1 structural coloration	7
3 Theory	9
3.1 Synthesis mechanism for RF derived carbon spheres.....	9
3.2 Activation of N-doping carbon spheres with phosphoric acid.....	10
3.3 Silica template method for enhancement of porosity	10
3.4 Characterization	11
3.4.1 Scanning Electron Microscope	11
3.4.2 Energy Dispersive X-ray Spectroscopy (EDS/EDX)	12
3.4.3 Nitrogen adsorption/desorption	12
3.4.4 Nanoparticle Tracking Analysis (NTA).....	12
4 Experimental	15
4.1 Optimizing morphology of the CS.....	15
4.1.1 Monodispersed RF resin spheres	15

4.1.2 Pyrolysis (carbonization) of RF spheres.....	16
4.2 Nitrogen doped carbon spheres.....	17
4.2.1 Nitrogen-doped RF spheres preparation.....	17
4.2.2 Carbonization of N-CS.....	17
4.2.3 Activation of N-CS with phosphoric acid (H ₃ PO ₄).....	17
4.3 Porous carbon sphere preparation using Si as template.....	18
4.3.1 Silica-RF spheres preparation.....	18
4.3.2 Carbonization of Silica-RF spheres.....	18
4.3.3 Removing silica template with potassium hydroxide (KOH).....	18
4.4 Characterization.....	19
4.4.1 SEM.....	19
4.4.2 EDS/EDS.....	19
4.4.3 Nitrogen adsorption/desorption.....	19
4.4.4 Nanoparticle Tracking Analysis.....	19
5 Result and discussion	21
5.1 Optimization of CS derived from RF polymer.....	21
5.1.1 Solvent composition.....	21
5.1.2 Initial temperature.....	23
5.1.3 Resorcinol and formaldehyde feeding molar ratio.....	24
5.1.4 Reaction time.....	26
5.1.5 Sonication Power.....	27
5.1.6 Concentration of the feeding reactants.....	29
5.1.7 Sum up the morphological optimization of synthesis parameters.....	30
5.2 N-CS result.....	31
5.2.1 Nitrogen introduction and morphology of N-CS.....	31
5.2.2 Size tuning of N-doped spheres with varying the catalyst concentration.....	32
5.2.3 N-CS with ethanol-free solvent.....	36
5.2.4 Specific surface area and porosity from BET.....	37
5.2.5 Activation of N-CS with phosphoric acid (H ₃ PO ₄).....	40
5.2.6 Yielding.....	42
5.2.7 Sum up N-CS.....	43
5.3 Result of Si-template modified CS.....	43
5.3.1 SEM.....	44
5.3.2 EDS.....	45

5.3.3 Structure properties(nitrogen adsorption/desorption) of Si-template Carbon spheres	46
.....
6 Conclusion	49
7 Future work	51
Bibliography	53
Appendices	A-1

LIST OF FIGURES

Figure 1 Emulsion polymerization synthesized RF-carbon micro-spheres size controlling by varying the condition parameters from Horikawa's study. (Horikawa, 2004)	4
Figure 2 Scheme of the formation of RF particles under sonication reaction	6
Figure 3 Schematic illustration of the multiple optical effects from photonic balls: (1) Bragg reflection; (2) grating diffraction; and (3) unselective scattering.	8
Figure 4: Proposed mechanism of RF polymerization under a basic catalyst	9
Figure 5 Schematics for the synthesis of nanoporous carbons: (1) polymerization of (RF) with silica nanoparticles; (2) carbonization of the RF gel/silica composite; (3)HF etching of silica	11
Figure 7 scheme of NTA.....	13
Figure 8 Milky solution consisted with PF spheres	16
Figure 9 scheme of carbonization program	17
Figure 10 SEM image with solvent composition variations	22
Figure 11 SEM image with initial temperature variations.....	23
Figure 12 SEM image with precursor concentration variations	25
Figure 13 Addition reaction of formaldehyde and resorcinol.....	25
Figure 14 SEM image with reaction time variations	27
Figure 15 SEM image with sonication power variations.....	28
Figure 16 SEM image with R/F variations	29
Figure 17 SEM image of (a),(b) obtained from (Vilas, 2014) (c),(d) from ours work; a), c) RF spheres; b), d) RF carbonization at 600 °C	31
Figure 18 SEM of N-doped CS with various R/M	32
Figure 19 SEM image of N-doped spheres prepared with various catalyst concentration	34
Figure 20 The scheme of (a) higher concentration of catalyst (b) lower concentration of catalyst, presented in the reactor. The black dots present catalyst and the grey dots present the R/F molecules.....	35
Figure 21 left) size distribution from NTA, right) SEM of N_RC_0.5	36
Figure 22 SEM image of N-doped spheres prepared without ethanol.....	37
Figure 23 BET isotherm for N_R/C_0.375_C750.....	40
Figure 24 SEM image of N-doped CS 1) polymer spheres 2) after carbonization 3) after H ₃ PO ₄ impregnation 4)after activation	41

Figure 25 SEM image of Si-template CS (left) before KOH etch (right) after KOH etch	44
Figure 26 EDS spectra of Si-template CS (left) before KOH etch (right) after KOH etch	45
Figure 27 EDS mapping of Si-template CS before KOH etch	45
Figure 28 EDS mapping of Si-template CS after KOH etch	46
Figure 29 BET isotherm of Si-template CS before KOH etch	47
Figure 29 SEM image of N_R/C_0.75 with marked scale	2
Figure 30 Size distribution from Nanosight of sample N_R/C_0.75.....	3
Figure 31 SEM image of N_R/C_0.5 with marked scale	3
Figure 32 Size distribution from Nanosight of sample N_R/C_0.5.....	4
Figure 33 SEM image of N_R/C_0.375 with marked scale	4
Figure 34 Size distribution from Nanosight of sample N_R/C_0.375.....	5
Figure 35 Size distribution from Nanosight of sample N_R/C_0.3.....	5
Figure 36 Size distribution from Nanosight of sample N_R/C_0.15.....	6
Figure 37 BET isotherm of sample N_R/C_6_C750.....	1
Figure 38 BET isotherm of sample N_R/C_1.2_C750.....	2
Figure 39 BET isotherm of sample N_R/C_0.75_C750.....	3
Figure 40 BET isotherm of sample N_R/C_0.5_C750.....	4
Figure 41 BET isotherm of sample N_R/C_0.375_C750.....	5
Figure 42 BJH Desorption dA/dD Pore Area analysis of Si_C750	6
Figure 43 BJH Desorption dA/dD Pore Area analysis of Si_C750_KOH	7

LIST OF TABLES

Table 1 Experimental parameters of samples for solvent composition studies	21
Table 2 Experimental parameters of samples for initial temperature studies	23
Table 3 Experimental parameters of samples for R/F studies	24
Table 4 Experimental parameters of samples for reaction time studies	26
Table 5 Experimental parameters of samples for sonication time studies	28
Table 6 Experimental parameters of samples for precursor concentration studies	29
Table 7 Experimental parameters of N-doped spheres for nitrogen uptake studies	32
Table 8 Experimental parameters of N-doped spheres for size tuning studies	33
Table 9 size of N-doped spheres prepared with various catalyst concentration	34
Table 10 Experimental parameters of N-doped spheres prepared water only solvent	37
Table 11 Experimental parameters of CS and N-doped CS at various carbonization temperature	38
Table 12 BET results of CS and N-doped CS	38
Table 13 BET results of N-doped CS with various catalyst concentration	39
Table 14 sample information of N-doped CS with H ₃ PO ₄ activation	41
Table 15 BET results of N-doped CS with H ₃ PO ₄ activation	42
Table 16 yielding of N-doped CS	42
Table 17 sample information of Si-template modified CS	43
Table 18 BET results of Si-template modified CS	47

LIST OF ABBREVIATIONS

Abbreviation

CS	Carbon Sphere
N-CS	Nitrogen doped Carbon Sphere
RF	Resorcinol and Formaldehyde
PMMA	Poly-Methyl Methacrylate
SEM	Scanning Electron Microscope
EDS/EDX	Energy Dispersive X-ray Spectroscopy
BET	Brunauer-Emmet-Teller
BJH	Barrett-Joyner-Halenda
NTA	Nanoparticle Tracking Analysis
XPS	X-ray photoelectron spectroscopy
ethOH	Ethanol
HCHO	Formaldehyde
H ₃ PO ₄	Phosphoric acid
KOH	potassium hydroxide
NH ₄ OH	Aqueous ammonia

Sample labeling abbreviations

RF_C	Resorcinol Formaldehyde Carbon sphere
N_C	Nitrogen doped Carbon sphere
Si_C	Silica-template modified Carbon sphere

1 INTRODUCTION

Monodispersed carbon spherical materials are attracting sustainable interesting not only due to their carbonaceous advantages, such as surface chemistry, excellent thermal properties, significant electrical conductivities and controllable pore structures, (Vilas, 2014) (Yang, 2014) but also their tunable spherical morphology, both in terms of the external size of the spheres and the internal porous structure. With these properties, the monodispersed carbon spheres will serve as promising materials for lots of applications such as adsorption, catalysis, drug delivery, photonic crystals, sensors, and energy storage/conversion. (Xia, 2000) (Tang, 2015)

There are lots of methods to synthesize the carbon spheres, including emulsion polymerization approach, hydrothermal and ultrasound-mediated methods, etc. The emulsion polymerization methods commonly used to generate micro-scale (50-1000 μ m) carbon spheres from aromatic precursor with certain surfactant in an emulsion solution. Nevertheless, the micro carbon spheres are less attractive than nano-spheres and limited in lots of applications due to their weak mechanical strength and size limitation. (Horikawa, 2004) (Peer, 2013) Until now, submicro and micro (200nm to 2 μ m) carbon spheres are successfully synthesized with hydrothermal approach by lots of groups. However, uniform dispersed carbon spheres are still rare to be found in those cases. (Qi, 2016) Furthermore, the energy and time consuming complex synthesis path is also a big challenge to scale up the production for both emulsion polymerization method and hydrothermal carbonization method. (LI, 2015) (Nilantha, 2014) Recently, Vilas and the other researchers (Alazemi, 2015) (Vilas, 2014) discovered an ultrasonic associated method for fast synthesis (within five minutes) of carbon spheres derived from resorcinol and formaldehyde (RF). It seems promising due to its simplicity and significant fast process.

In order to further maximize the application potential of the monodispersed carbon spheres, lots of modification has been investigated, (Tang, 2015) including physical and chemical structures improvements. The physical structures mainly include morphology, particle diameters, specific surface area, pore volume, pore diameter distribution, etc. The chemical

structures mainly include the type of surface functional groups (generally, oxygen, nitrogen, phosphoric groups, etc.), acidic-basic properties, hydrophilic-hydrophobic properties, and metal/metal oxides doping etc. (Yang, 2014). By far, N-doped porous carbon spheres has been intensively studied due to its excellent performance in drug delivery, oxygen reduction reaction, supercapacitors, CO₂ capture and Li-S batteries. However, the complex and costly synthesis path may hinder the production and application of N-CS. Thus a less complex and cost friendly synthesis method is urgently required. (Ferrero, 2016)

In this work, 1) In order to consistently produced the highly ordered, or monodispersed carbon spheres, this project systematically studied the effect of synthetic parameters (e.g. catalyst concentration, solvent composition, ultrasonic power, ultrasonic time, reaction temperature, and precursor concentration) on the morphology of the spheres, mainly the roundness and size distribution. 2) The uniform N-CS were designed to synthesize from melamine, formaldehyde and resorcinol with sonication method. Size tuning of N-CS particle, from nano-range to micro-range, is conducted by varying the catalyst concentration. The activation of N-CS is studied using H₃PO₄ as activation agent. The surface texture and porosity of N-CS were also investigated in this work. 3) The silica nanoparticles are used as hard template for modifying the porous property of the carbon spheres. All above work and the results obtained will give valuable guidance to the synthesis and structure control of carbon spheres by the ultrasonic mediated method.

2 LITERATURE REVIEW

2.1 Development and outlook of monodispersed sphere

Truly monodispersed spheres have been first produced by Stöber (Stöber, 1968) procedure of by the hydrolysis and condensation of tetraethyl orthosilicate assisted by ammonia catalyst in 1968. Such monodispersed silica particles, ranged from 50nm to 200 μm , offer many experimental and theoretical advantages such as facilitating simple calibration procedures for analytical equipment and simplify the data analytical process. Moreover, the availability of the monodispersed sample is also the key to achieve homogeneous, crystalline arrays with larger range, which will lead to a broad range of brilliant applications such as drug delivery, structural coloration, energy storage, sensor and catalytic support. (Xia, 2000) (Sun, 2013)

However, the systematic studies about monodispersed spheres have not been well developed yet. The limited diversity of the monodispersed materials and the little control of the morphology are the main challenge now. By far, only silica and a few polymers (e.g. polystyrene and PMMA (poly-methyl methacrylate) have been successfully produced as truly monodispersed colloidal spheres. These materials may be less attractive because of lacking of certain functionalities like optical, electrical properties. (Xia, 2000) Unlike polymer and silica materials mentioned above, carbon- based materials exhibit good electronic conductivity and chemical stabilities, which will significantly expand the applications of the monodispersed spheres if truly uniform carbon spheres become available. (Horikawa, 2004)

2.2 Different approaches of carbon sphere synthesis

2.2.1 Emulsion polymerization

The emulsion polymerization method is used to generate carbon spheres from aromatic precursor with certain surfactant in an oil-in-water emulsion. Horikawa produced CS with this method using resorcinol and formaldehyde as carbon source and successfully control the

size from 50-1000 μm , as showed in figure 1. Generally, the emulsion polymerization approach usually prepared the carbon sphere in a micrometer range. It is difficult to synthesize the carbon spheres with sizes below 10 μm . (Horikawa, 2004) The CS prepared by the emulsion polymerization method, is highly sensitive to the precursor recipe, oil/water ratio, surfactant type and concentrations, stirring rate, and etc. which make it difficult to have a good control of the final product. In addition, the polymer spheres prepared by the emulsion polymerization approach easily failed to be converted into their carbonaceous analogues because of thermal decomposition. Thus, the application of emulsion polymerization approach was limited. (Peer, 2013)

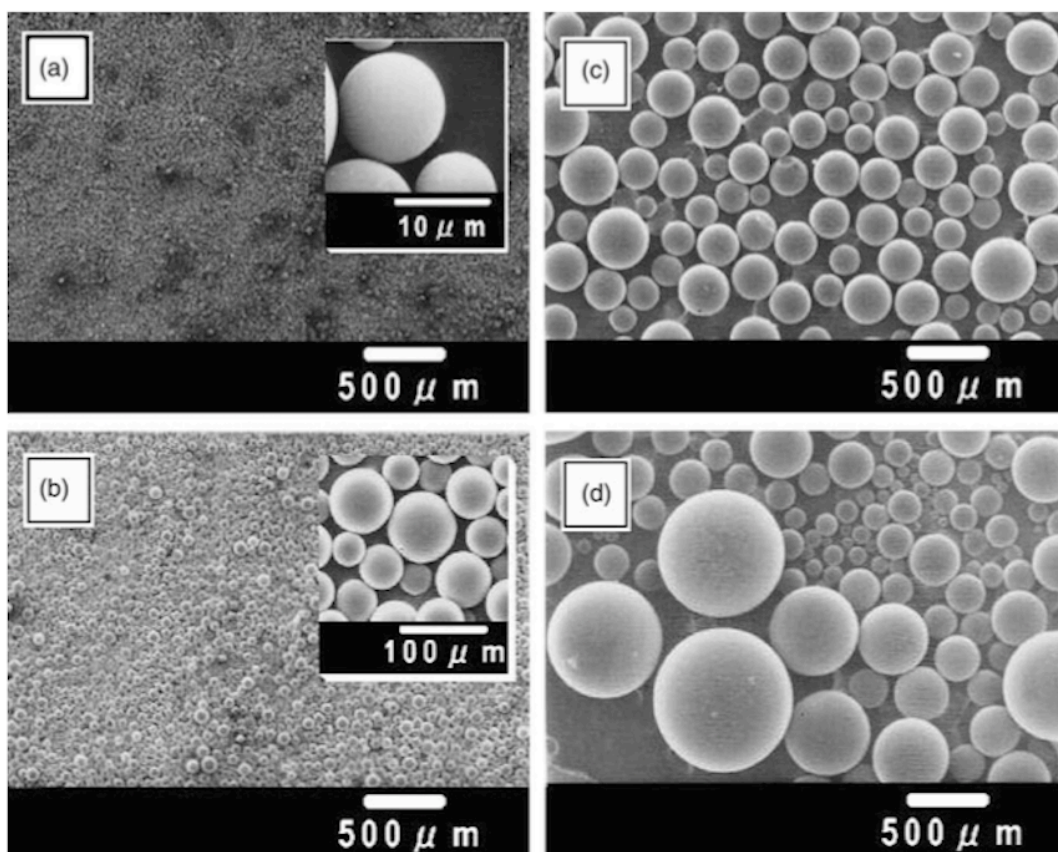


Figure 1 Emulsion polymerization synthesized RF-carbon micro-spheres size controlling by varying the condition parameters from Horikawa's study. (Horikawa, 2004)

2.2.2 Hydrothermal approach

Hydrothermal method is a method used to crystallize the reactants with high temperature aqueous solutions at high vapor pressure. It is widely used method to prepare the carbon spheres by carrying out in an autoclave. (Deshmukh, 2010) With this method, the size of carbon spheres can be tuned within the range of 50-1000 nm (LI, 2015). Ordered porous

carbon spheres can also be synthesized by the soft-template assisted hydrothermal method. (Liu J. , 2013) The pore structure and surface chemistry (such as nitrogen doping) are easily tuned by adjusting the recipe of the precursor, the catalyst and surfactant types and concentration, and hydrothermal synthesis process parameters (e.g. temperature, heating rate, holding time, etc.). It is noted that hydrothermal method can also be used for carbon sphere synthesis from biomass-derived precursors (e.g. glucose, cellulose, xylose, starch, and so on.). This will make the synthesis of carbon sphere in a very cheap and sustainable way. (LI, 2015) (Nilantha, 2014). However, the hydrothermal method is a time and energy consuming process, generally, hydrothermal temperature for the carbon sphere synthesis is in the range of 100-200°C and the hydrothermal duration is usually more than 8 hours. Thus, the high procedure costs become the main challenge of applying hydrothermal method to scale up the CS production. It is highly desired to find a facile and rapid method to synthesize the carbon sphere. (LI, 2015) (Nilantha, 2014)

2.2.3 Untrasounds irradiation method

Vilas reported a more efficient rapid and cost friendly way to generate monodispersed RF spheres within five minutes by using ultrasound irradiation method instead of hydrothermal approach. The scheme of his synthesis process is illustrated in the Figure 2. The sonochemical effect is the key for rapid formation of RF spheres. Ultrasound irradiation generates extreme high temperature and pressure, result from continuous nucleation, bubble growth and impulsive collapse of bubble in the solution. The high pressure and temperature not only provide enough energy for water dissociate into H• and OH• radicals, which initiate the polymerization of resorcinol and formaldehyde but also facilitate all the chemical reactions in the systems. It has been proved that the submicro-scaled RF spheres can be successfully synthesized by this sonication method. However, the nano-scaled particles or hetero-atom doped carbon spheres have not been investigated using this method. (Vilas, 2014) (Alazemi, 2015)

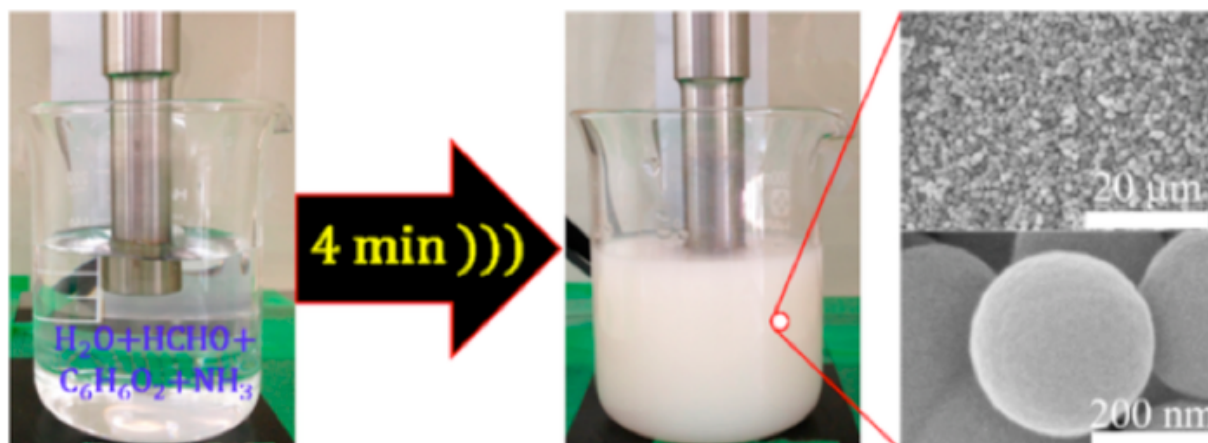


Figure 2 Scheme of the formation of RF particles under sonication reaction

2.3 Nitrogen doped carbon spheres

N-CS has attracted considerable attention due to its excellent performance in drug delivery, oxygen reduction reaction, supercapacitors, CO₂ capture and Li-S batteries. (Ferrero, 2016). The introduction of heteroatom into the carbon is aimed to modify the chemical properties of the CS. As showed in the Figure 3, nitrogen atoms are generally mixed into carbon materials in the form of pyridinic-N, graphitic-N and pyrrolic N-C. (Wei, 2015)

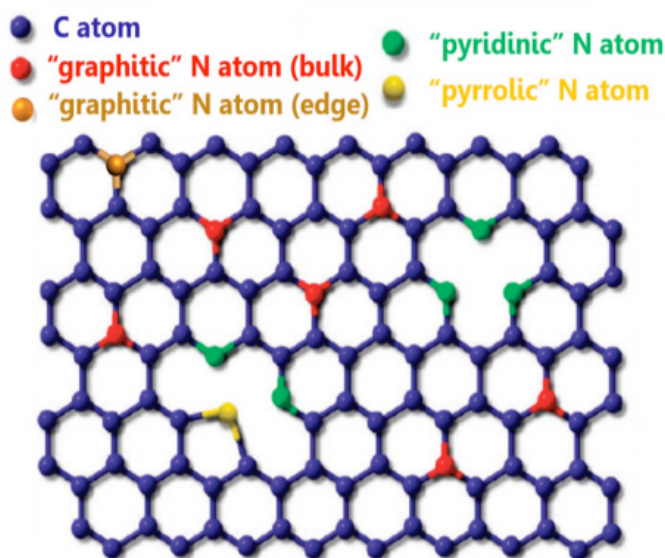


Figure 3 Scheme of carbon network with doped Nitrogen group

Many studies (Zhang, 2012) (Ewert, 2015) (Wickramaratne, 2014) reported that nitrogen containing carbon showed a significant improvement of selectivity and chemical adsorption capacity for CO₂ capture due to the incorporation of basic nitrogen groups ensure an enhanced

adsorption of acidic gas like CO₂. In terms of supercapacitors, a tremendous enhancement of the capacitance has been witnessed. The mechanism behind these enhancement has not been fully understood. However, several studies (Liu X. , 2014) (Ewert, 2015) proposed that the nitrogen, with extra electron in the outer layer, altered the electronic structure of the carbon matrix and leads to a better surface polarity, electric conductivity and thus larger interfacial capacitance. Also, the nitrogen doping creates lots of defected site, as demonstrated in the Figure 3, leading to the improvements of lithium intercalation properties. (Wei, 2015)

There are usually two approaches for the synthesis of nitrogen contained porous carbon materials.

- 1) Using of nitrogen-containing source as starting precursor.
- 2) Post treatment of carbon materials with ammonia and urea at elevated temperature.

The first method is applied in this work and it is also most commonly used in the industry mainly because of its simplicity and feasibility. The second method is more complicated and can easily destroy the original structure of the pre-treated carbon material.

2.4 Application of carbon spheres

2.4.1 structural coloration

Material properties can be significantly influenced by the way how molecules or nanoparticles with different structures and morphologies assemble themselves into certain pattern in the nanoscale. Unlike the color we usually think of, obtained by pigment absorbing the certain wavelength of the light (visible light 400nm-800nm) and reflecting the rest of the wavelengths. Structure color, like the stunning hues of a butterfly's wings or a peacock's tail, result from the objective's micron and nano-structured periodic pattern that constructively or destructively reinforcing or canceling out the specific wavelengths of the visible lights. That's why our eyes can conceive that iridescent color of the butterfly wings.

Sphere is the one of most promising candidates to construct the designed structure because it can easily self-assemble into designed pattern attributing to their unique and perfectly symmetrical geometrical properties. The photonic balls built up from closely stacked nanoparticles is a great example of how the spheres can produce structural color without any pigments. (Venugopal, 2015) As demonstrated in the figure 4, the photonic ball generate: 1) bright spot, 2) rainbow light, 3) white light. The three different lights caused by three main modes of interactions between light and structured balls: 1) Bragg reflection (it happens when the light hit highly ordered structure like the ordered packed spheres showed here or most of the crystal), 2) and grating diffraction (light hits a periodic structure with small gaps, which splits and diffracts the light into different color beams) and 3) unselective scattering (normal

light which conceived as white because of unselective scattering caused by unordered structure). (Kinoshita, Yoshioka, & Miyazaki, 2008)

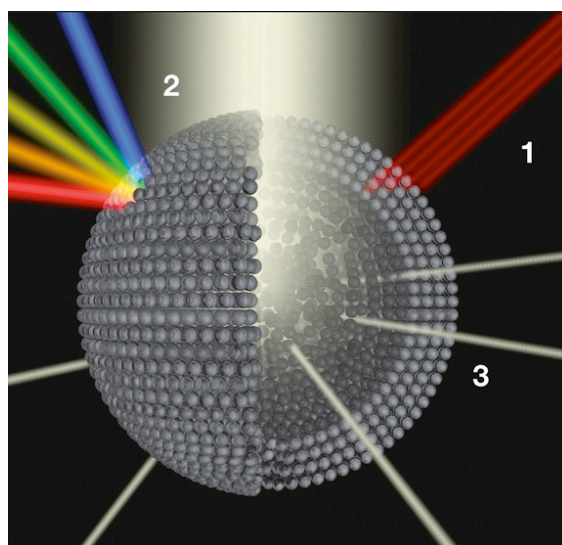


Figure 4 Schematic illustration of the multiple optical effects from photonic balls: (1) Bragg reflection; (2) grating diffraction; and (3) unselective scattering.

By manipulating the packing and the structure of the spheres we can get different color in various forms which can wildly apply in many areas. Furthermore, compared with the traditional color dyeing materials, which has lots of drawbacks like they usually generating lots of toxic pollution during production process and the traditional dyeing materials often fade out after certain amount of time, the structural coloring material is more environmental friendly and also more advanced in a sustainable way.

3 THEORY

3.1 Synthesis mechanism for RF derived carbon spheres

Among various carbon sources, RF polymer is most commonly used carbon precursors for carbon sphere production. The carbon materials can be obtained by pyrolysis of RF polymer in an inert gas at a various temperature, generally from 600-1000°C. The proposed mechanism of RF polymerization is illustrated below in Figure 5. First, a base catalyzed addition reaction of resorcinol and formaldehyde forms methylol resorcinols, these methylol compounds subsequently undergo a condensation reaction with each other to form nano-cluster then further crosslink to a gel network. (Elkhatat, 2011)

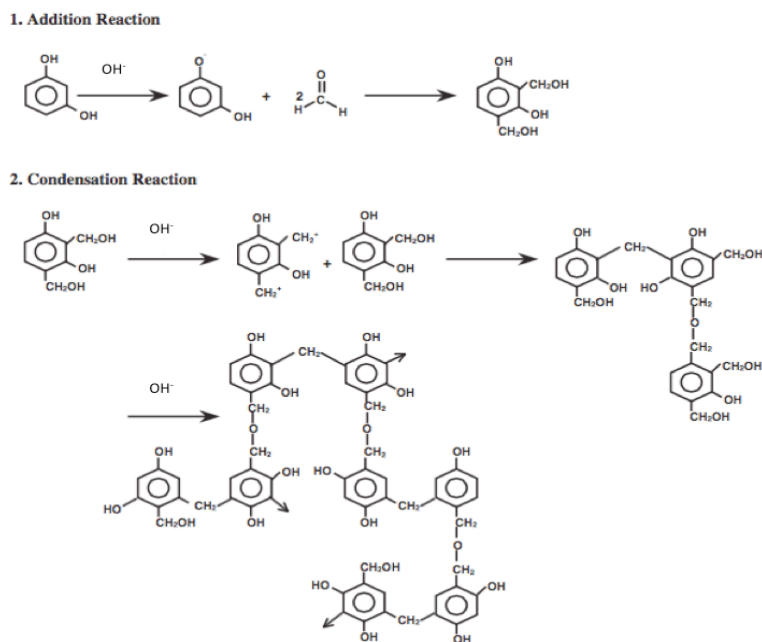


Figure 5: Proposed mechanism of RF polymerization under a basic catalyst

3.2 Activation of N-doping carbon spheres with phosphoric acid

The carbon spheres generated from pyrolysis of RF resin has limited pore volume, specific surface area and limited pore size range, generally only micropores are achieved from carbonization. Therefore, proper activation is necessary to modify the porous property of the CS.

Physical and chemical activations are basically two mainly methods for carbon activation production. Physical activation uses steam and carbon dioxide to active the pre-carbonized materials and usually carbonization and activation are carried out separately. Chemical activation use H_3PO_4 , potassium hydroxide (KOH) or $ZnCl_2$ to mix with carbon materials, followed by carbonization/activation thermal treatment at a temperature ranging from 500 to 900°C. (Kim, 2004)

The carbon activation with KOH and H_3PO_4 (Wang, 2012) are two of the most commonly used method to achieve high specific surface area and defined pore volume distribution. However, the disadvantage of using KOH is the lower yielding of activated carbons and destruction of the structure of the carbons due to its high corrosion capacity. On the other hand, the H_3PO_4 usually used for activating biomass carbons with a higher carbon yielding and more controllable structure after activation. (olawale, 2011) The structure destruction of our spheres is one of the biggest concern about using strong activation reagent, therefore, a less strong activation reagent, H_3PO_4 is picked up for this study to ensure the intact spherical shape.

3.3 Silica template method for enhancement of porosity

Porous materials can be categorized into microporous (pore diameter less than 2nm) mesoporous (pore diameter between 2nm to 50nm) and macroporous (pore diameter lager than 50nm), according to their pore size. Microporous material has a better performance of capturing and storing small molecules like inorganic molecules and ions. Additional, micropores has a relative slow releasing rate for the drug delivering. However, it may also cause unwanted mass transform limitation if only micropores are presented in the material. (Wickramaratne, 2014) In order to solve this mass transform limitations, additional mesopores and macropores are desired for expending porous CS applications. (Ewert, 2015) The main challenge of conventional porous carbon materials is that it has little control of the pore size distribution. (Ewert, 2015) Therefore, carbon materials with a controllable hierarchical porosity ranging from micropores through mesopores to macropores may significantly enhance the properties and the applications of the material. Hard template

method is the most commonly used approach to achieve designed porous carbon materials. (Lee, 2004)

Generally, as showed in Figure 6, the synthesis of carbon materials with ordered porous by using hard template (e.g. silica nanoparticles) includes these steps: 1) preparing silica gel with designed pore structure, 2) infiltration of the silica template into the polymer precursor, 3) gelation and carbonization of the polymer 4) dissolution of the silica template. The schematic illustration is showed in Figure 6 . (Lee, 2004)

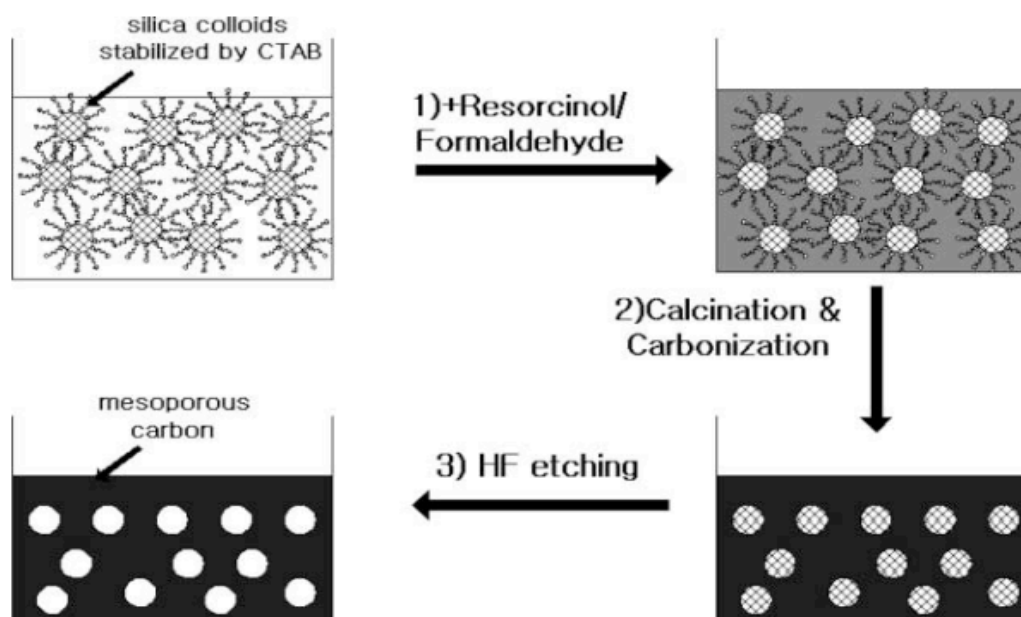


Figure 6 Schematics for the synthesis of nanoporous carbons: (1) polymerization of (RF) with silica nanoparticles; (2) carbonization of the RF gel/silica composite; (3) HF etching of silica

3.4 Characterization

3.4.1 Scanning Electron Microscope

Scanning Electron Microscope (SEM), as an electron microscope, is usually applied to study the morphology and topology of the sample by obtaining an image of the objective. The high-resolution images (nanoscale) are achieved by scanning the sample with focused electronic beams. The scanning electrons interact with the atoms in the sample, emitting various electrons due to different electron collision mechanisms. The electron detector subsequently collects the scattered electrons. The two most commonly detected scattered electrons are secondary electron and back-scattered electrons. When the primary electron hits the sample, the sample absorbs this primary electron and emits another electron with less energy due to

the collision mechanism, this emitted electron with less energy called the secondary electron. The back-scattered electron is generated by the reflection collision of the primary electron with the sample. These detected scattered electrons are finally processed by the analytical system to generate the high-resolution image of the sample. (McMullan, 1988)

3.4.2 Energy Dispersive X-ray Spectroscopy (EDS/EDX)

Energy Dispersive X-ray Spectroscopy(EDS) is used to analyze the elements in the tested sample. Similar to SEM, EDS also relies on the interaction of the X-ray excited electrons or protons, or a beam of X-rays with the sample atoms. The interaction usually causes the specific energy emission of the attacked atom from the specimen, which can be further analyzed energy-dispersive spectrometer. Because of each atom's unique atomic structure, the corresponded X-ray spectroscopy can be distinguished from each other, which leads to the availability of the elements analysis from EDS. (Goldstein, 1992)

3.4.3 Nitrogen adsorption/desorption

Nitrogen adsorption/desorption is usually applied to obtain the textural properties of texted material such as surface area, pore volume, pore size distribution and etc. by using the knowledge of the physical adsorption and desorption on the material's surface based on some surface theories, most commonly, Brunauer-Emmet-Teller theory which based om Langmuir theory. BET method, the most common method, obtains the surface area by measuring the volume of the gas adsorbed at the surface, at a constant temperature (77K liquid nitrogen), as a function of the equilibrium pressure. The pressure is demonstrated as a relative pressure: actual pressure p divided by the vapor pressure. Pore volume and pore diameter can be determined using the Barrett-Joyner-Halenda(BJH) method. The BJH desorption data are used in this paper to obtain the pore size of the material, interpreting as the certain amount of the adsorbate (nitrogen) lost at different pressure, which means the occupied pores are then emptied at the responding pressure. Combining with the Kelvin equation and some adsorption/desorption assumptions, pore volume and pore diameters can be calculated. (webb, 2002)

3.4.4 Nanoparticle Tracking Analysis (NTA)

NTA applied to obtain the particle size distribution of the samples in liquid suspension by utilizing both the light scattering and Brownian motion.

As demonstrated in Figure 7, a laser beam is used by passing through the sample chamber, which is filled with liquid suspension containing our sample particles, to make the particles more easily visualized under a magnification microscope coupled with a video camera. The camera captures a video file of particles moving caused by Brownian motion. The NTA software subsequently tracks down the captured particles individually and calculates their size using the Stokes-Einstein equation. (Malvern, 2016)

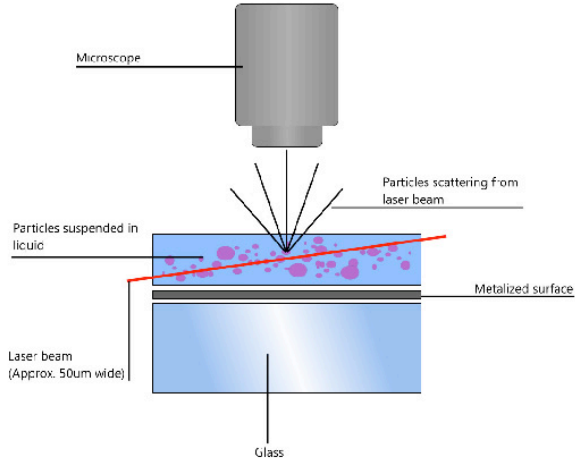


Figure 7 scheme of NTA

4 EXPERIMENTAL

4.1 Optimizing morphology of the CS

4.1.1 Monodispersed RF resin spheres

The experimental method used to prepare different monodispersed spheres in this work is based on the Stöber 's method and Vilas's method. (Stöber, 1968) (Vilas, 2014) However, in an attempt to duplicate Vilas' CS, many of our experiment failed to generate monodispersed spheres consistently by following their method. In order to stably produce monodispersed CS, systematically studies of discovering how the reaction parameters effect the morphology of the CS had been conducted in here.

Sonication reaction

First, ethanol (96v%) solution and deionized water were mixed in a 250ml beaker. Aqueous ammonia (NH₄OH 25wt%) solution served as catalyst was added and well mixed into the ethanol-water solvent. Solid resorcinol (99%, Sigma-Aldrich) and formaldehyde (37wt% in aqueous solution stabilized by 10% methanol, Sigma-Aldrich) are mixed into the solution for ultrasounds irradiation (SONOPULS HD 3200, 200W, Bandelin, Germany).

After starting the ultrasonication, the color of the solution in the reactor changed from transparent through peachy orange to milky color in the end, which shows in the Figure 8.

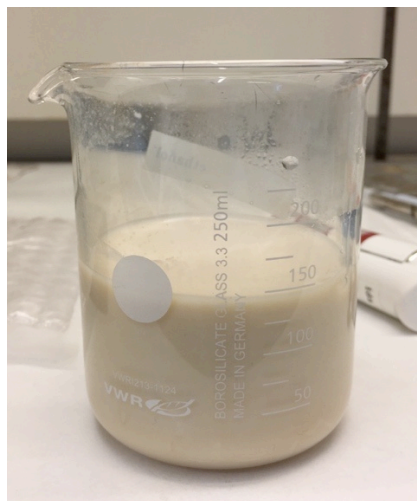


Figure 8 Milky solution consisted with PF spheres

Sample recovering

First, solid product is separated from the milky solution by centrifugation (1100rpm for 20minutes). Secondly, gently wash the separated spheres to remove residue ammonia by using ethanol (96 v%) solution. Ultrasonic bath is subsequently applied to give a homogeneous distribution of the spheres in the ethanol solution for a better wash. Continuously washing, ultrasonic bathing and centrifugating the sample for 3 times. The separated solid sample was dried in the fume hood over night. Finally, the pure RF resin spheres were vacuum dried at 40°C for 4 hours. Weighting the sample after the recovering, recording the weight.

4.1.2 Pyrolysis (carbonization) of RF spheres.

The spherical RF resins were carbonized in an inert atmosphere (nitrogen). A typical thermal treatment program used in this work is showed here: purging inert gas for 30minutes to remove the air inside the carbonization tube, then heating the RF spheres to 600-900 °C, with a 1.5 degree per minute heating ramping, such a low heating rate is aimed at protecting the morphology of the spheres. After holding the final temperature for 3 hours, cooling the samples to room temperature with a rate of 10 °C per minute.

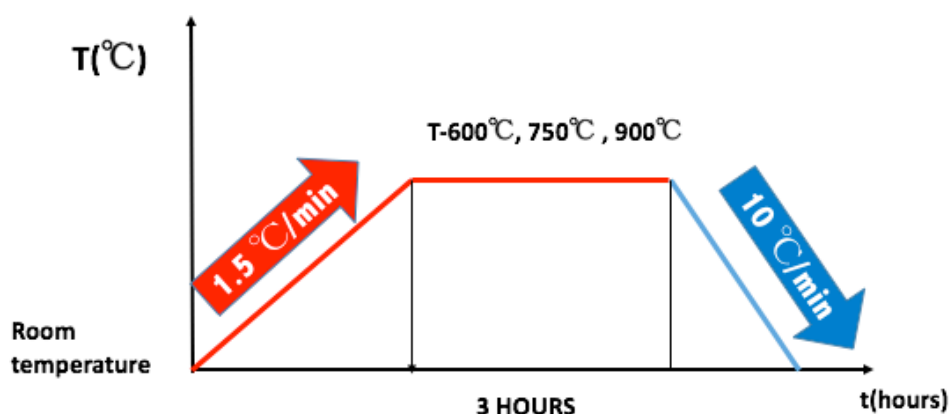


Figure 9 scheme of carbonization program

4.2 Nitrogen doped carbon spheres

4.2.1 Nitrogen-doped RF spheres preparation

Mixing 40ml ethanol (96v%) solution, 100ml deionized water and 1ml formaldehyde (37wt%) in a 250ml beaker. Different amount of ammonia (NH₄OH 25wt%) solution was added to catalyze the reaction and tune the size of the particles. Designed specific amount of Melamine (99%, Sigma-Aldrich) and Resorcinol were added into the beaker for ultrasounds irradiation at a 30% power for 5minutes.

The rest of the recovering steps are the same as RF sphere preparation described before.

4.2.2 Carbonization of N-CS

The N-CS carbonization program is the same as the RF spheres, which has described in details before. Weighting the sample both before and after the carbonization.

4.2.3 Activation of N-CS with phosphoric acid (H₃PO₄)

200mg of nitrogen contained carbon spheres were impregnated with 20 ml of phosphoric acid solutions (3mol/L) then stirred at 85 °C, maintaining for 4 h to ensure the access of H₃PO₄ to

the interior of the carbon spheres. Drying the well mixed sample at room temperature for at least 12 hours. Thermal activation was carried out in a vertical tubular furnace at 900°C under nitrogen gas protection.

4.3 Porous carbon sphere preparation using Si as template

4.3.1 Silica-RF spheres preparation

First, 40ml ethanol (96v%) solution and 100ml deionized water were prepared as solvent. Second, 1g solid resorcinol and 0.75ml aqueous ammonia (NH₄OH 25wt%) solution were added and well mixed into the ethanol-water solvent. Finally, 0.65ml silica colloid (LUDOX SM 30wt%, Sigma-Aldrich) and 1ml formaldehyde (37wt%) are mixed into the solution for ultrasounds irradiation at a 30% power for 5minutes.

The rest of the recovering steps are the same as RF sphere preparation described above.

4.3.2 Carbonization of Silica-RF spheres

Flowing the nitrogen gas for 30minutes to remove the air inside the carbonization tube, then heating the RF spheres to 600 and 750 °C individually, with a 1.5 °C per minute heating ramping. After holding the final temperature for 3 hours, cooling the samples to room temperature with a 10 °C per minute rate.

4.3.3 Removing silica template with potassium hydroxide (KOH)

100mg carbonized Si-RF carbon spheres were impregnated with 10ml potassium hydroxide solution (5mol/L) in a flask. Keep the flask in the oil bath at 80°C for 12 hours. Carefully wash the sample with deionized water and separate the products with centrifugation (9000rpm, 20minutes) to remove the residual KOH, repeat the wash process for 3 times. Product was dried in the oven (120°C) for at least 6 hours.

4.4 Characterization

4.4.1 SEM

The morphology and topology are studied using the Hitachi S-5500 in lens cold field emission Scanning transmission electron microscope (S(T)EM), with a secondary electron(SE) detector.

The acceleration voltage was set from 7kv to 30kv for different samples, and beam current was set to be 10 μ A. All the samples were mounted on a carbon tape before testing.

4.4.2 EDS/EDS

The elements mapping was obtained by Bruker EDX-system attached with S(T)EM. The optimized Bruker EDX-system allows the mapping measurements and analysis completed within a couple of minutes.

4.4.3 Nitrogen adsorption/desorption

Nitrogen adsorption/desorption was performed with a Tristar 3000 Surface area and Porosity Analyser device from Micrometrics. Prior to analysis, all samples were degassed in 200 $^{\circ}$ C for 12 hours in a VACPREP 061 sample degas system. The sample tube was immersed in the liquid nitrogen to obtain a constant temperature at 77K.

4.4.4 Nanoparticle Tracking Analysis

The size analysis of the particles was performed with the Malven NanoSight LM 10 instrument. Before injecting the liquid sample into the testing laser chamber, a proper diluting process should be conducted to ensure the concentration of the particles is in the testing range described in the user's manual.

5 RESULT AND DISCUSSION

5.1 Optimization of CS derived from RF polymer

The various experimental parameters listed below were systematically studied to uncover the relationship between reaction condition and the morphology of the RF spheres.

1. Solvent composition
2. Initial temperature
3. Resorcinol and formaldehyde feeding molar ratio
4. Reaction time
5. Ultrasonic power
6. Reactant concentration

5.1.1 Solvent composition

We first explored the effect of solvent composition on the morphology by using different solvent with various water to total (water and ethanol) volumetric ratio. The sample information is listed in Table 1, sorted by decreasing the water content.

Table 1 Experimental parameters of samples for solvent composition studies

	HCHO (ml)	Resorcinol (g)	Water (ml)	EtOH (ml)	NH₄OH (ml)	Initial T(°C)	Power (%)	Reaction time (min)
RF_W100%	1.4	1	140	0	0.5	25	80	5
RF_W70%	1.4	1	100	40	0.5	25	80	5
RF_W60%	1.4	1	85	55	0.5	25	80	5
RF_W50%	1.4	1	70	70	0.5	25	80	5

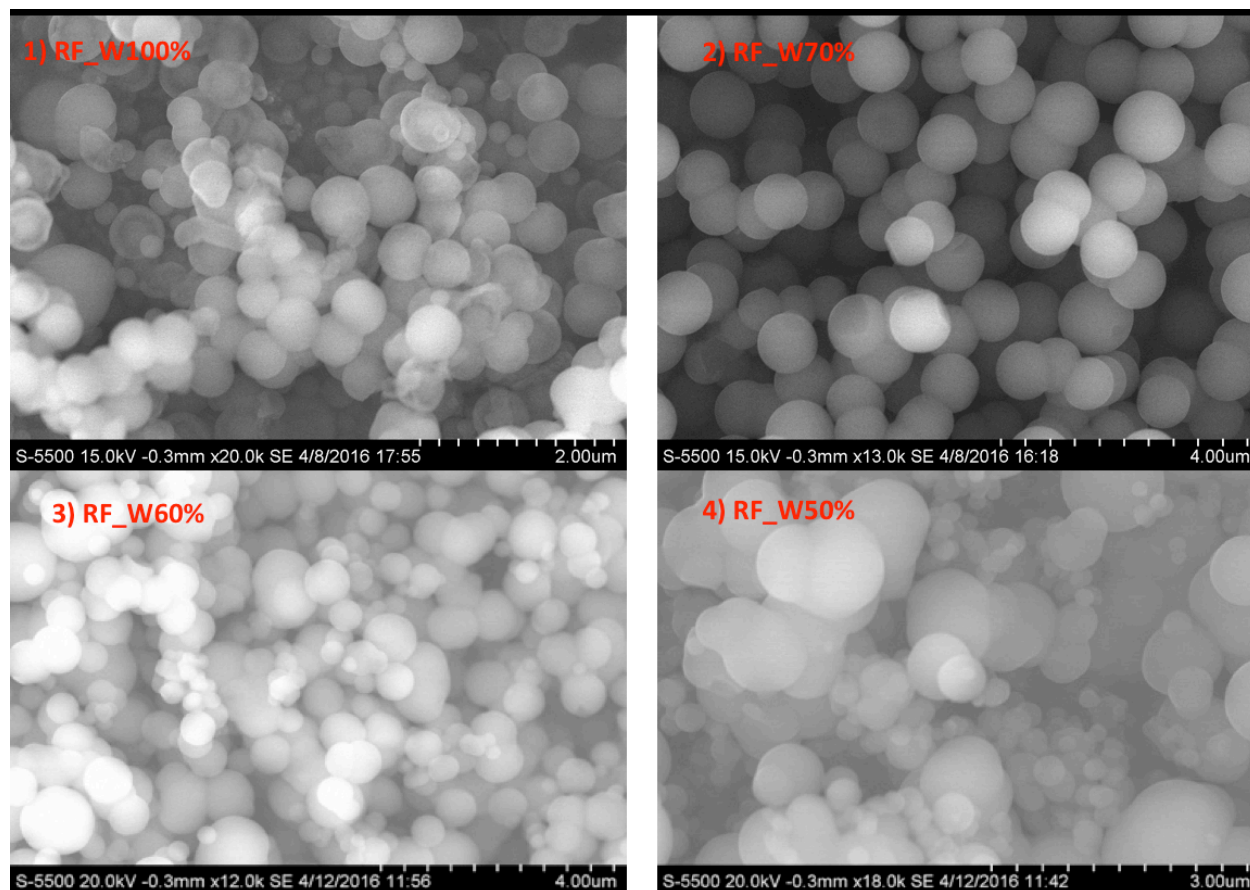


Figure 10 SEM image with solvent composition variations

As figure 10 shows, sample prepared with 100 ml water and 40 ml ethanol, denoted as RF_W70%, shows the best morphology in terms of spherical roundness. Starting from the water-only case denoted as RF_W100%, the additional ethanol mixed in the solvent improves the roundness of the RF spheres. However, the spheres turned into coarse and irregular shape again if sequentially adding more ethanol into the solvent.

In summary, the morphology of the spheres shows the sensitivity to water to ethanol ratio in the solvent, the water to ethanol ratio can be optimized for a better performance of the sphere synthesis.

As many groups (Elkhatat, 2011)(Peer, 2013) reported, the 100ml water to 40 ml ethanol ratio is the most used composition when making the RF resin materials, which also confirmed with our experiment. The mechanism underneath this phenomenal is not well understood yet, but it might be that ethanol can improve the dispersion of the feeding components when serving as an organic solvent in the reaction with an optimized quantity, however, too much ethanol may hinder the polymerization inside the reactor.

5.1.2 Initial temperature

Initial temperature was also studied here to explore the effect of temperature on the morphology. The temperature is always changing during the process due to the significant heat released from the sonication reaction. Therefore, the initial temperature is measured to identify the temperature variance of the samples. The initial temperatures of 15°C, 25°C, and 40°C were achieved by using an ice bath; no bathing (room temperature) and heating the solvent by ultrasonic irradiation until 40°C, respectively. The sample information is listed in Table 2, sorted by increasing the initial temperature.

Table 2 Experimental parameters of samples for initial temperature studies

	HCHO (ml)	Resorcinol (g)	Water (ml)	EtOH (ml)	NH₄OH (ml)	Initial T(°C)	Power (%)	Reaction time (min)
RF_T15	1.4	1	100	40	0.5	15	80	5
RF_T25	1.4	1	100	40	0.5	25	80	5
RF_T40	1.4	1	100	40	0.5	40	80	5

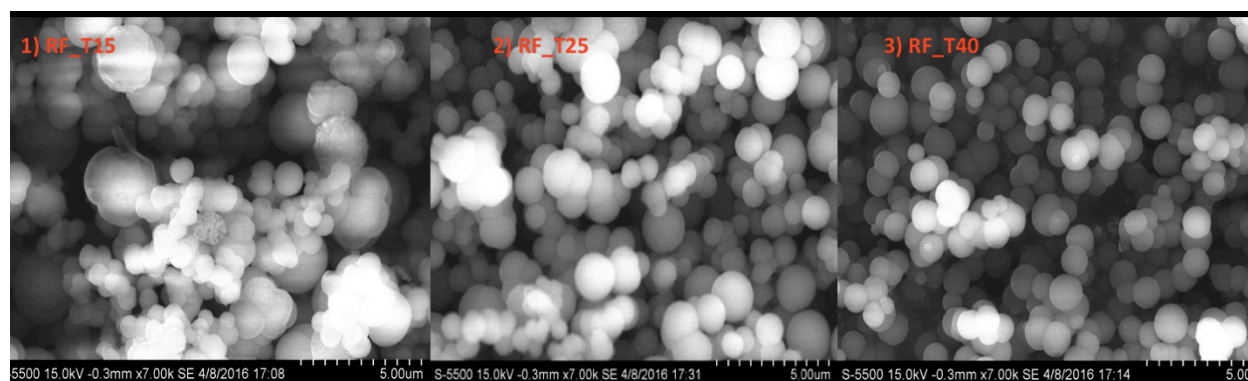


Figure 11 SEM image with initial temperature variations

The SEM images of different samples with different initial temperatures are shown in Figure 11. The ice-bathing batch, denoted as RF_T15, gave the widest size distribution. In the other hand, with increasing the initial temperature to 25°C, (RF_T25) the sample shows a significant improvement on narrow size distribution. Nonetheless, the size distribution didn't achieve more improvement as further increasing the initial temperature to 40°C.

The poor morphology caused by using ice bath may be explained by the huge temperature gradient from the center of beaker, where the ultrasonic probe located, though the solution to the wall of the beaker, contacted with the ice bath. Recall from the theory chapter, the high pressure and high temperature ultrasonic irradiation releasing significant amount of heat in the sonication bubbles. (Vilas, 2014). Thus the temperature in the center of the reactor will maintain a relative higher temperature, while the relative lower temperature presented near the wall of the beaker caused by the ice bath. As some research groups (Blaha, 2013) (Stejskal, 1998) stated that temperature has particular impact upon polymerization process. Specifically, higher temperature leads to faster polymerization. In other words, the temperature gradient inside the solution leads to different polymerization rate, which subsequently results in various sizes of the synthesized spheres.

According to Figure 11, RF_T25 and RF_T40, almost have the same performance regarding the size distribution, which confirms that the temperature is not actually the reason for wider size distribution but the temperature gradient inside the reactor is the main affects for size distribution. Thus, homogenous temperature distribution inside the reactor can narrow the size distribution of the synthesized spheres when using the ultrasounds method.

5.1.3 Resorcinol and formaldehyde feeding molar ratio

The effect of resorcinol to formaldehyde molar ratio (R/F) on the spheres was explored in here by varying the formaldehyde mass feeding while keeping the resorcinol feeding constant. The sample information is listed in in Table 3. sorted by increasing the R/F molar ratio, in other word, decreasing F mass feeding.

Table 3 Experimental parameters of samples for R/F studies

	HCHO (ml)	Resorcinol (g)	Water (ml)	EtOH (ml)	NH₄OH (ml)	Initial T(°C)	Power (%)	Reaction time (min)
RF_R/F_1:2	1.4	1	100	40	0.5	25	80	5
RF_R/F_3:5	1.2	1	100	40	0.5	25	80	5
RF_R/F_7:8	1	1	100	40	0.5	25	80	5
RF_R/F_1:1	0.8	1	100	40	0.5	25	80	5

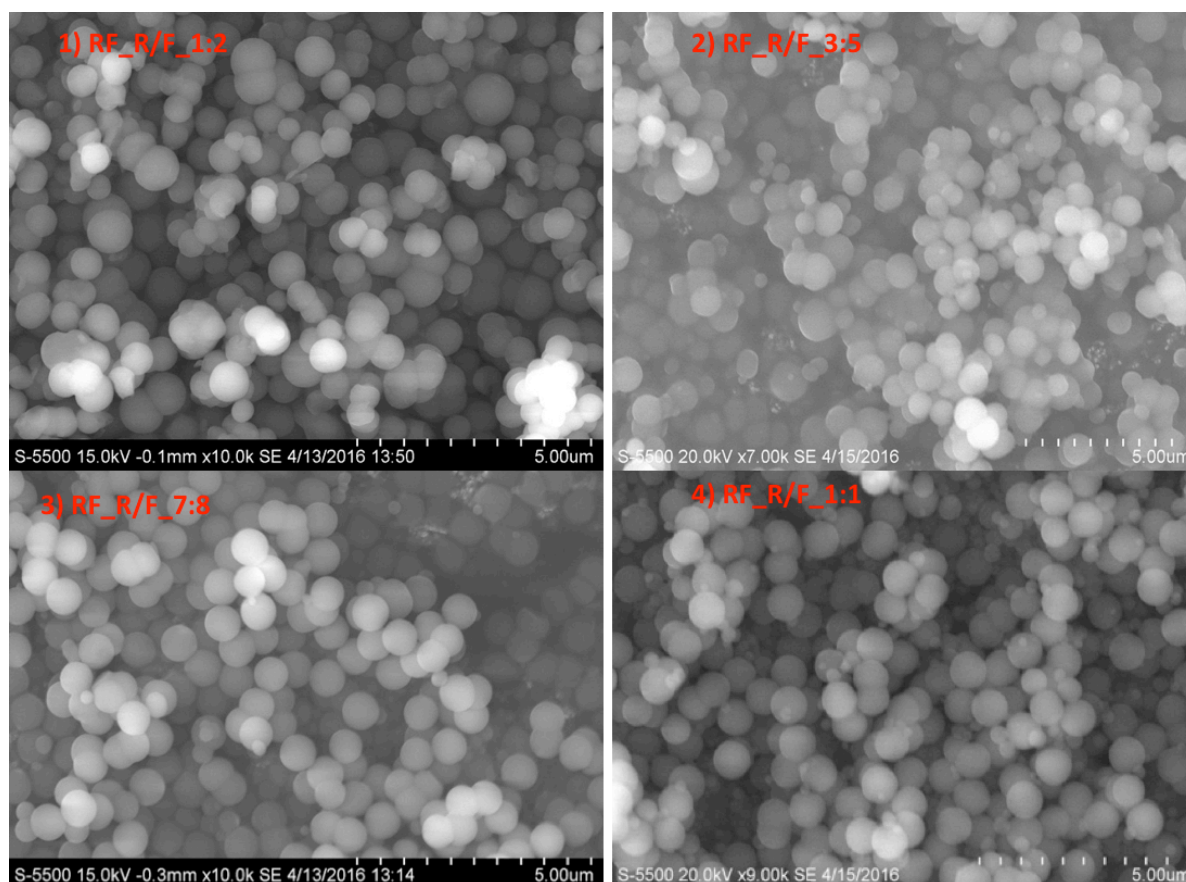


Figure 12 SEM image with precursor concentration variations

According to Figure 12, the sample prepared with a R/F ratio of 1:2 gives more irregular shape, broader size distribution and more aggregation cluster between the particles. The spheres obtained better roundness and narrower size distribution with decreasing the amount of the formaldehyde until the R/F ratio reaches 7:8. However, it starts to generate considerable amount of small spheres among the bigger spheres, if further decrease the formaldehyde content to a R/F ratio of 1:1.

In summary, the R/F ratio of 7:8 offers the best spherical shape and almost monodispersed spheres, in addition, not noticeable aggregation is observed.

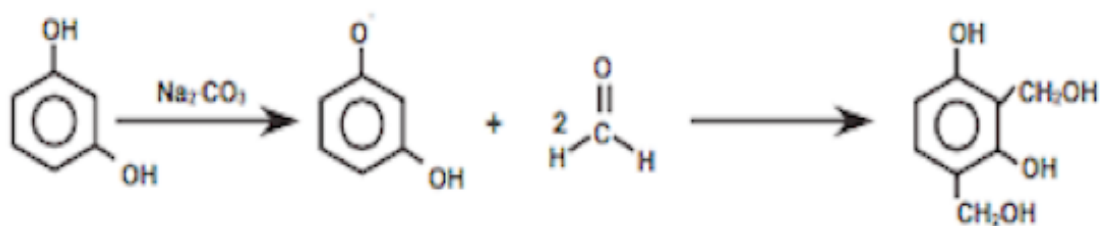


Figure 13 Addition reaction of formaldehyde and resorcinol

The various morphology obtained from SEM in Figure 12, indicates that the roundness and size distribution of the spheres are significant sensitive to the R/F ratio, thus monodispersed spheres can be obtained by optimizing the R/F ratio. Usually, the R/F molar ratio is set to be 1:2, since for one Resorcinol(1,3-dihydroxybenzene) is capable of adding two formaldehyde (HCHO) in the 2-, 4-, and/ or 6- positions of its aromatic ring when having the addition reaction with formaldehyde. Then the condensation reaction will take place. (Al-Muhtaseb, 2003) The proposed reaction mechanism of addition reaction is showed in the figure 13. for a basic catalytic RF polymerization. (Al-Muhtaseb, 2003). To best our knowledge, the effects of R/F molar ratio on morphology of the CS have not been addressed yet. In here, we propose that it may be the geology feature of the spherical shape demands specific R/F molar ratio, namely, such a spherical structure may require an optimized R/F ratio to fit in the spherical polymeric matrix.

It is worth mention, the RF_R/F_7:8 is the first batch we have ever made that comprised with almost monodispersed spheres. For future reference, the spheres synthesized after this serious were all prepared with a R/F ratio of 7:8.

5.1.4 Reaction time

Varying reaction time is simply by sonication the reaction for different time span. Sample information is listed in Table 4, sorted by increasing the reaction time.

Table 4 Experimental parameters of samples for reaction time studies

	HCHO (ml)	Resorcinol (g)	Water (ml)	EtOH (ml)	NH₄OH (ml)	Initial T(°C)	Power (%)	Reaction time (min)
RF_3min	1	1	100	40	0.5	25	80	3
RF_5min	1	1	100	40	0.5	25	80	5
RF_15min	1	1	100	40	0.5	25	80	15

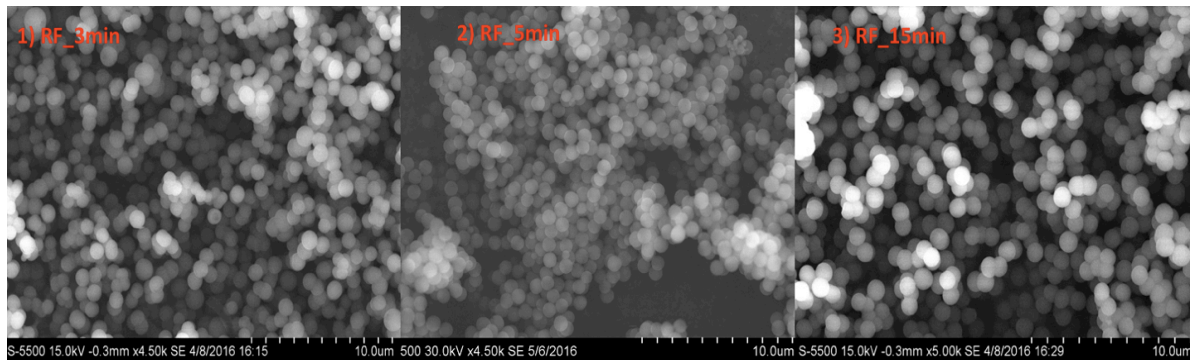


Figure 14 SEM image with reaction time variations

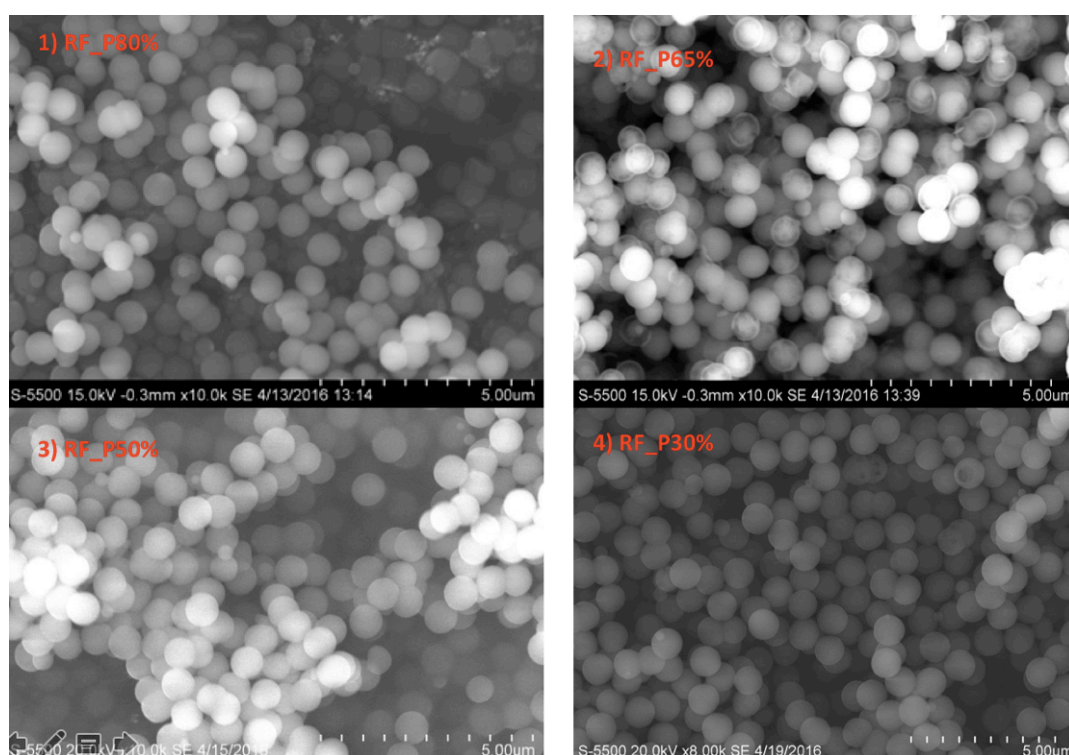
According to Figure 14, all three samples show uniform size distribution and good spherical shape, indicating that the variation of sonication duration didn't show dramatic effects on the shape nor the size of the RF resin spheres. Vilas group (Vilas, 2014) also observed the similar phenomenon by varying reaction time from 5 minutes to 1 hour. Longer reaction time did not result in any effects on size and shape might be explained by the limited reactants in the reactor, namely, almost all the reactants has already been consumed after roughly 5 minutes' sonication, thus further sonication doesn't give any theatrical effect upon the size or the shape of the spheres. (Horikawa, 2004) It is worthy notice that various sonication duration can cause various temperature in the reactor, longer sonication result in higher temperature while shorter sonication result in lower temperature. Thus, the different temperature inside the reactor does not give noticeable effects on the morphology of the RF spheres, which also confirmed by the temperature gradient proposal in the "Initial temperature effects" studies.

5.1.5 Sonication Power

Various sonication power (80%, 65%, 50%, 30% of the full power, full power of the sonication device is 200W) had been conducted in this section to study how the ultrasonic power effect the morphology of the RF spheres. Sample information is listed in Table 5, sorted by decreasing the sonication power.

Table 5 Experimental parameters of samples for sonication time studies

	HCHO (ml)	Resorcinol (g)	Water (ml)	EtOH (ml)	NH ₄ OH (ml)	Initial T(°C)	Power (%)	Reaction time (min)
RF_P80%	1	1	100	40	0.5	25	80	5
RF_P65%	1	1	100	40	0.5	25	65	5
RF_P50%	1	1	100	40	0.5	25	50	5
RF_P30%	1	1	100	40	0.5	25	30	5

*Figure 15 SEM image with sonication power variations*

According to Figure 15, all the samples in this series show good roundness and relative narrow size distribution. However, the samples prepared with higher power such as RF_P80% and RF_P65% show some aggregated spheres, which represented as two or three merged together in the SEM figure 15. The sample prepared with lower power, denoted as RF_P30%, shows less agglomerated spheres.

In brief, this may be explained by the surface free energy, in other words, higher sonication power provides extra energy for the particles to merge with each other via reactions among the surface functional group. (Peer, 2013) (Qi, 2016) Therefore, a lower power and thus lower energy can reduce the adhesion of the spheres in the solution.

5.1.6 Concentration of the feeding reactants

Different concentration of the feeding reagents is obtained by adjusting the feeding mass of both formaldehyde, resorcinol and total volume of the solvent.

Sample information is listed in Table 6, sorted by decreasing the R/S (S represents solvent) ratio.

Table 6 Experimental parameters of samples for precursor concentration studies

	HCHO (ml)	Resorcinol (g)	Water (ml)	EtOH (ml)	NH ₄ OH (ml)	Initial T(°C)	Power (%)	Reaction time (min)
RF_R/S_2	2	2	100	40	0.5	25	30	5
RF_R/S_1	1	1	100	40	0.5	25	30	5
RF_R/S_0.67	1	1	150	60	0.5	25	30	5

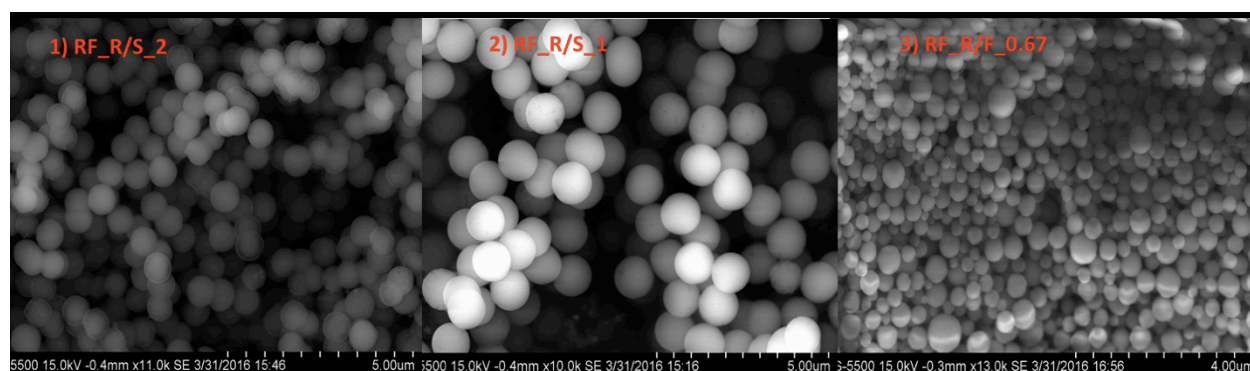


Figure 16 SEM image with R/F variations

In Figure 16, all three samples in the series present relative good spherical shape. Specially, the RF_R/S_1 has remarkable performance not only the perfectly spherical shape but the highly narrowed size distribution.

RF_R/S_2, prepared with doubling both the concentration of the resorcinol and the formaldehyde, shows slightly more aggregated spheres. This is reasonable since higher concentration means higher chance that two or more spheres would interact with each other in a more crowded situation. (Nilantha, 2014) (Peer, 2013)

RF_R/S_0.67, prepared by adding 50v% more solvent into the reactor, presents good roundness but wider size distribution. It may result of the bigger temperature gradient caused from larger volume of solvent, which means less homogenous distributed heat generated by

ultrasonication probe. As mentioned before, the sonication probe was placed in the center of the reactor, thus the temperature in the center may be slightly higher than the area far away from the center. Therefore, the temperature gradient will become bigger if the total volume of the solvent is larger, simply because the edge of the solution became further away from the center.

Briefly sum up, the lower concentration of the feeding reagent may give a less agglomerated RF spheres.

5.1.7 Sum up the morphological optimization of synthesis parameters

Briefly sum up the optimized parameters, the morphology of the RF sphere is significantly sensitive to R/F molar ratio, solvent composition and temperature gradient. Optimizing these three parameters is the key to stably generating uniform sized smooth spherical spheres. Lower sonication power may reduce the aggregation of the spheres. Reaction time and feeding concentration seem to have less effect on the morphology of the spheres. Specific optimized parameters are listed here: R/F molar ratio, water to total solvent percentage and the sonication power are set to be 7:8, 70v% and 30%, respectively, in room temperature(25°C).

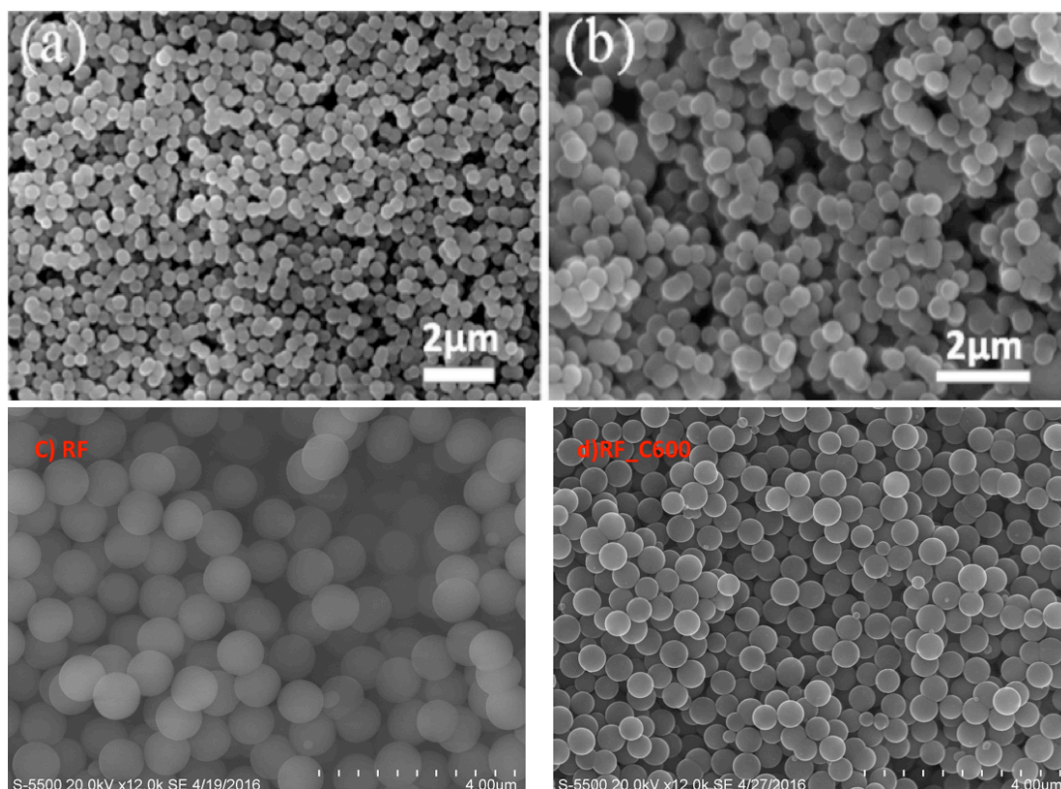


Figure 17 SEM image of (a),(b) obtained from (Vilas, 2014) (c),(d) from ours work; a), c) RF spheres; b), d) RF carbonization at 600 °C

Purely monodispersed well separated PF resin spheres are stably maintained by optimizing the experimental parameters in this section. In Figure 17. It shows the spheres optimized by our work on the bottom (c) (d) and the ones prepared by the Vilas group on the right (a) (b)(Vilas, 2014). It's clearly, the spheres have been improved by us both in terms of spherical shape and the narrow size distribution.

5.2 N-CS result

5.2.1 Nitrogen introduction and morphology of N-CS

This series of samples are prepared to study the relationship between introduced nitrogen content and the morphology of the spheres. The content of the melamine is commonly studied by varying the resorcinol to melamine (R/M) molar ratio. Lower R/M ration represents higher melamine concentration. The sample information is listed in Table 7

Table 7 Experimental parameters of N-doped spheres for nitrogen uptake studies

	HCHO (ml)	Resorci nol (g)	Melam ine (g)	Water (ml)	EtOH (ml)	NH ₄ O H (ml)	Initial T(°C)	Powe r %	Reactio n time (min)
N_R/M_0.5	1	0.33	0.76	100	40	0.75	25	30	5
N_R/M_1	1	0.50	0.57	100	40	0.75	25	30	5
N_R/M_2	1	0.67	0.38	100	40	0.75	25	30	5

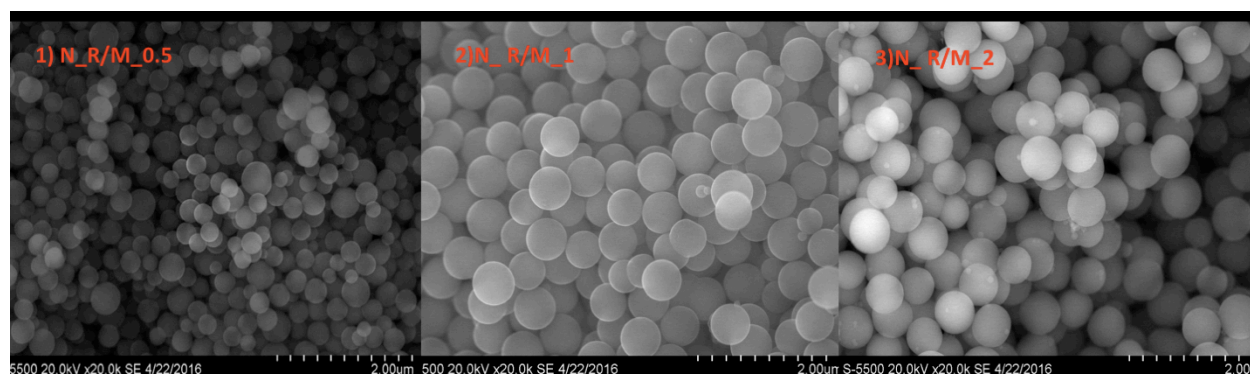


Figure 18 SEM of N-doped CS with various R/M

According to Figure 18, all the three samples show good spherical shape. R/M_0.5, with highest melamine content presents the broadest size distribution. R/M_1 and R/M_2 present similar narrow size distribution. It is also noticed that the N-doped spheres with a higher nitrogen feeding concentration, N_R/M_0.5, yields a smaller spherical size.

The catalyst concentration can have a drastic impact upon the size of the spheres, higher catalyst concentration gives smaller spherical size. Some articles reported (Sharma, 2009; Bazargan, 2013) that this may explain by the alkalinity of the melamine, the basic melamine may change the pH of the solution resulting some effecting of the polymerization. Based on other studies (Liu X. , 2014) (Nilantha, 2014), the higher melamine feeding leads to higher nitrogen uptake in the final spheres. Thus, it was decided to keep the R/M ratio as 1:1 for the later N-doped spheres' preparation. In this way, we can obtain a good spherical shape and a narrow distribution without compromising losing significant amount of nitrogen element in the spheres.

5.2.2 Size tuning of N-doped spheres with varying the catalyst concentration

In order to elucidate the effect of catalyst concentration on the size of the N-doped spheres, different N-doped spheres are prepared with various catalyst concentration. The concentration

of the catalyst is commonly studied by varying the resorcinol to catalyst (R/C) molar ratio. Lower R/C ration represents higher catalyst concentration. The sample information is listed in Table 8, sorted with increasing the catalyst concentration.

Table 8 Experimental parameters of N-doped spheres for size tuning studies

	HCH O (ml)	Resorcino l (g)	Melamin e (g)	Wate r (ml)	EtO H (ml)	NH₄O H (ml)	Initia l T(°C)	Powe r %	Reactio n time (min)
N_R/C_6	1	0.50	0.57	100	40	0.25	25	30	5
N_R/C_2	1	0.50	0.57	100	40	0.75	25	30	5
N_R/C_1.2	1	0.50	0.57	100	40	1.25	25	30	5
N_R/C_0.75	1	0.50	0.57	100	40	2	25	30	5
N_R/C_0.5	1	0.50	0.57	100	40	3	25	30	5
N_R/C_0.37	1	0.50	0.57	100	40	4	25	30	5
5									
N_R/C_0.3	1	0.50	0.57	100	40	5	25	30	5
N_R/C_0.15	1	0.25	0.28	100	40	5	25	30	5

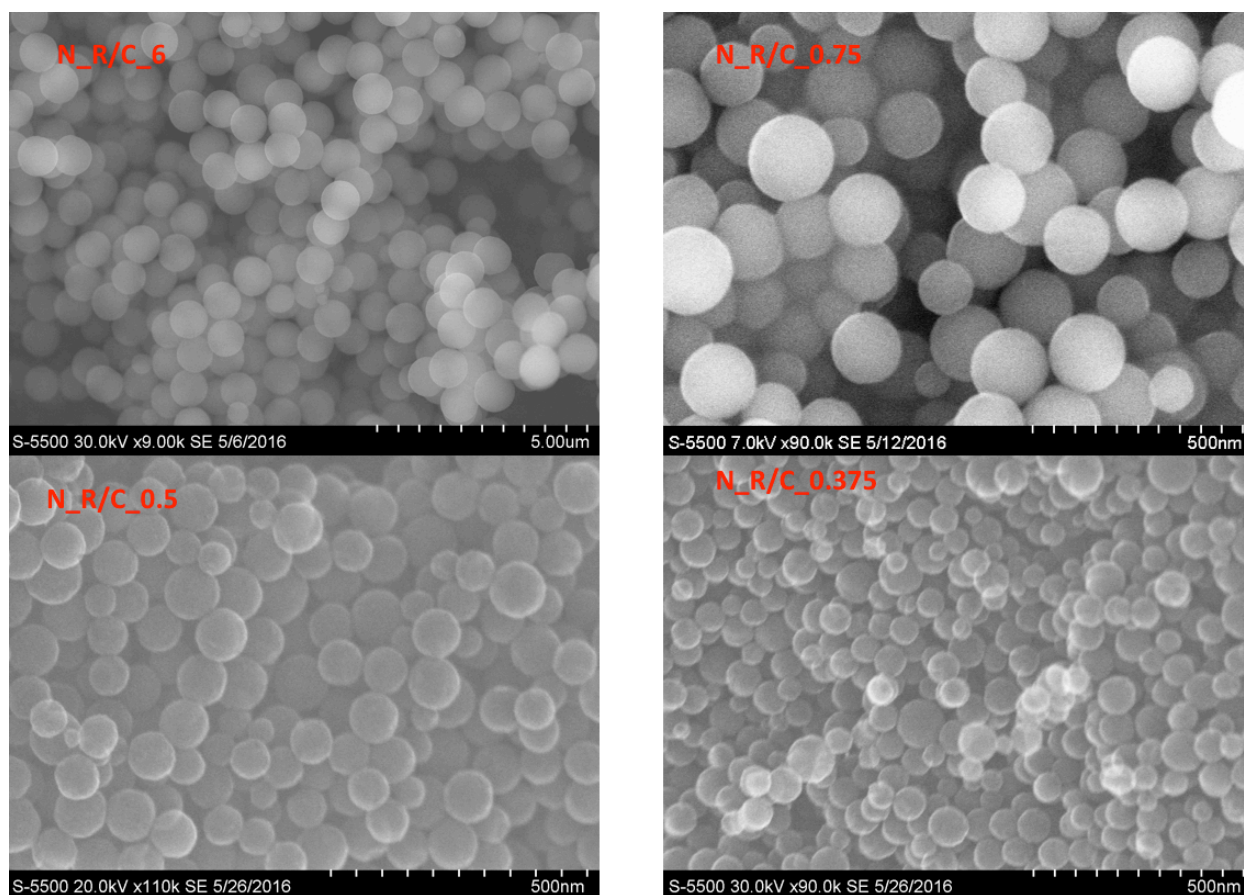


Figure 19 SEM image of N-doped spheres prepared with various catalyst concentration

The Table 9. shows the sizes of various sample, the samples are sorted with decreasing the R/C molar ratio, in the other words, with increasing the catalyst concentration.

Table 9 size of N-doped spheres prepared with various catalyst concentration

	Size estimated from SEM (nm)	Hydrodynamic size from Nano-sight (nm)
N_R/C_6	800	
N_R/C_2	600	
N_R/C_1.2	300	
N_R/C_0.75	170	175
N_R/C_0.5	90	105
N_R/C_0.375	60	75
N_R/C_0.3		55
N_R/C_0.15		45

According to Figure 19. and the data gathered from Nano-sight in Table 9, show that the sizes of most of the samples (N_RC_0.75, N_RC_0.5, N_RC_0.375, N_RC_0.3, N_RC_0.15) are below 200nm. Inspiringly, a sub 50nm range is obtained for sample N_RC_0.15. This is to

say, there is a drastic drop in the size by simply increasing the concentration of the catalyst in the solution. The SEM image in Figure 19, clearly shows the spherical size has been successfully tuned from submicro-scale to nano-scale. Good spherical shape has been obtained and no obvious agglomerating has been observed.

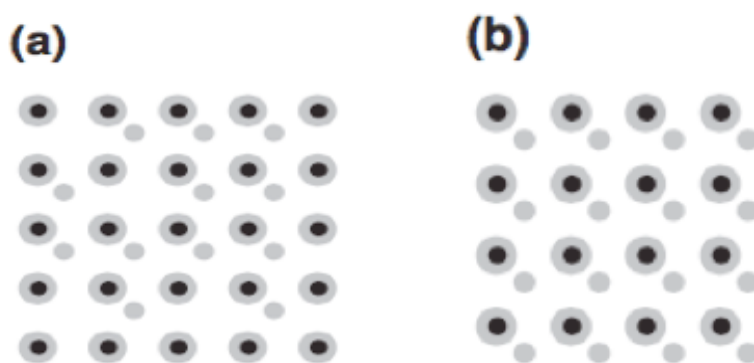


Figure 20 The scheme of (a) higher concentration of catalyst (b) lower concentration of catalyst, presented in the reactor. The black dots present catalyst and the grey dots present the R/F molecules.

There are two proposals to elucidate this effect. 1) As illustrated in the scheme Figure 20: the sample with higher concentration of catalyst has more available spots for nucleation, which result in less nucleation growth (smaller size) in each spots when same amount of R and F reagents are fed into the solution. 2) Recall the mechanism from polymerization chemistry, when H^+ and OH^- (or H^\bullet and OH^\bullet) concentration below a critical concentration, the free radicals mostly contribute to the initiation step. However, with increasing the basic catalyst concentration in the reaction, the free radical concentration overcome that critical concentration, the extra free radicals start to take part in the termination step, which directly leads to less developed polymerization, in other word, smaller polymer size. (Peer, 2013) (Deshmukh, 2010)

It is inspiring that the size tuning (from 1 micrometer to 50 nanometer range) has been successfully completed simply by manipulating the concentration of the catalyst (aqueous ammonia) in the solution.

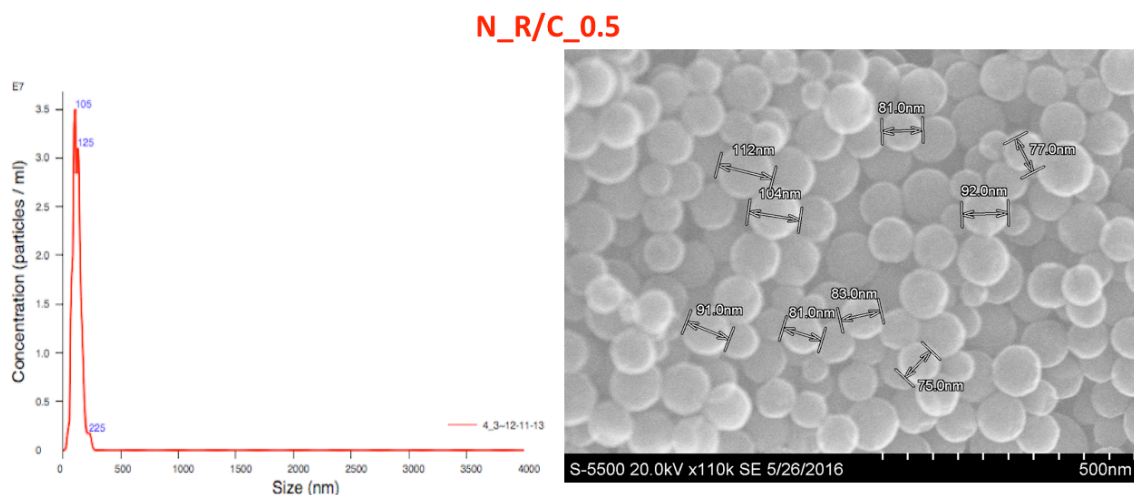


Figure 21 left) size distribution from NTA, right) SEM of N_RC_0.5

As illustrated in Figure 21 and Table 9, The size data of some samples (e.g. N_R/C_0.75, N_R/C_0.5 AND N_R/C_0.375) are collected from both SEM and Nano-sight. The data for bigger spheres (bigger than 50nm) are estimated from SEM, because the Nanosight can not correctly measure the particle whose size is bigger than 200nm. For smaller spheres, the data were estimated from the data collected with Nanosight. It is worthy notice, the size measured from Naonosight is hydrodynamic size, resulting from the dissolving of the spheres in the water before the measurements. The hydrodynamic size or volume might be certain degree larger than the drying size or volume. As showed in the figure 21, the SEM shows an estimated average diameter of 90nm while the measurement from the Nanosight reported 120 nm as the average size. Briefly, the data collected from Nanosight and the SEM are all estimated size data, which can only be used to analyze the general trend of the size.

5.2.3 N-CS with ethanol-free solvent

Alcohol, generally ethanol, mixing with water is most commonly used solvent for preparing uniform sphere. Some reach group stated that the alcohol to water volumetric ratio and the different type of alcohol had profound impact on the morphology of the polymer spheres. In some cases, the absence of ethanol in the solvent might lead to the failure of production of polymer spheres. (Peer, 2013) (Deshmukh, 2010). However, the tedious water-alcohol separation procedure not only consuming significant amount of energy and time, but also maybe a potential pollution for environment. In here, we dedicate to probe an alcohol-free synthesis method for N-CS by adjusting the condition parameters, without compromising the morphology of the spheres.

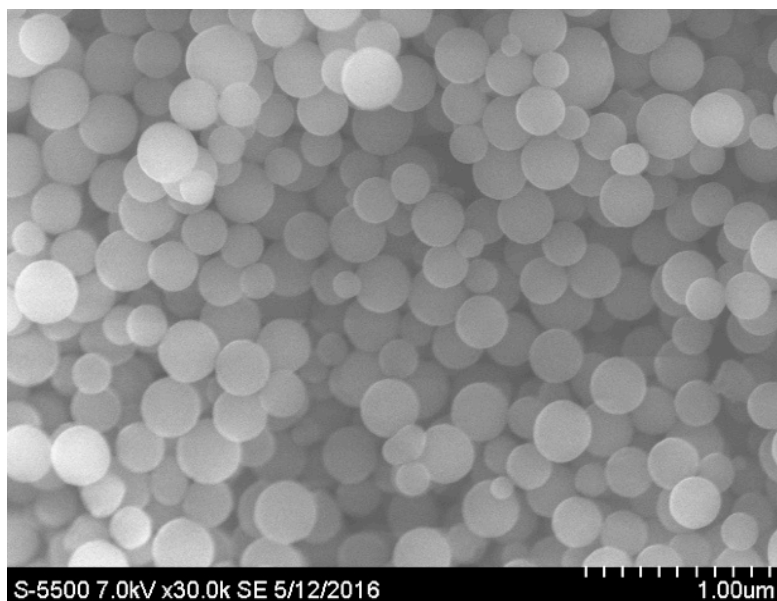


Figure 22 SEM image of N-doped spheres prepared without ethanol

The SEM image of the N-doped sphere prepared with ethanol-free solvent, Figure 22 shows good spherical shape, no distinct cohesion between the spheres, which indicates that we successfully synthesized the N-doped spheres by only water as solvent. The experimental parameters of this N-doped sample prepared are listed in table below.

Table 10 Experimental parameters of N-doped spheres prepared water only solvent

	HCHO (ml)	Resorcinol (g)	Melamine (g)	Water (ml)	EtOH (ml)	NH ₄ OH (ml)	Initial T(°C)	Power %
N_W100%	1	0.50	0.57	140	-	0.75	25	30

5.2.4 Specific surface area and porosity from BET

5.2.4.1 RF carbon spheres Vs. N-CS

This series of samples tested by nitrogen adsorption and desorption, to investigate the effect of doped nitrogen element on the surface texture and porous construction of the CS after various carbonization temperature(600, 750, 950 °C). Sample information has been listed in table 11, in order to have a better comparison of RF spheres and N-doped spheres, the samples are sorted in the pair of RF spheres and N-doped spheres.

Table 11 Experimental parameters of CS and N-doped CS at various carbonization temperature

	HCH O (ml)	Reso rcino l (g)	Mela mine (g)	Water (ml)	EtOH (ml)	NH ₄ O H (ml)	Initial T(°C)	Powe r %	Carboniz ation T (°C)
RF_C600	1	0.50	-	100	40	0.75	25	30	600
N_RF_C600	1	0.50	0.57	100	40	0.75	25	30	600
RF_C750	1	0.50	-	100	40	0.75	25	30	750
N_RF_C750	1	0.50	0.57	100	40	0.75	25	30	750
RF_C900	1	0.50	-	100	40	0.75	25	30	900
N_RF_C900	1	0.50	0.57	100	40	0.75	25	30	900

Table 12 BET results of CS and N-doped CS

	Surface area _{BET} (m ² /g)	Pore volume _{micro} (m ³ /g)	Pore volume _{tot} (m ³ /g)
RF_C600	411.0	0.186	0.215
N_RF_C600	458.8	0.211	0.237
RF_C750	502.8	0.229	0.260
N_RF_C750	579.9	0.261	0.304
RF_C900	543.9	0.246	0.288
N_RF_C900	583.4	0.264	0.313

According to Table 12, all the samples show that microporosity is contributing the most of the total pore volume, namely, the carbon spheres derived from both RF spheres and N-doped RF spheres are microporous spheres. On the other hand, both the surface area and pore volume increase slightly after nitrogen doping for different carbonization temperature. Compared with RF carbon spheres, the surface area of N-doped spheres increases 11.6%, 15.3% and 7.3% for carbonization temperature at 600°C, 750°C and 900°C, respectively. The total pore volume increases 10.2%, 16.9% and 8.7% for carbonization temperature at 600°C, 750°C and 900°C, respectively.

As mentioned in theory, the microporosity of the CS and N-CS after carbonization are both due to the escaped heteroatoms (e.g. hydrogen, oxygen and/or nitrogen atom, in N-CS case) at

high temperature treatment. It is inspiring that comparing with CS, the N-CS does slightly increase the surface area and pore volume after carbonization at all different carbonization temperature. The mechanism under this is not well understood, however some studies proposed that, nitrogen (structured with 5 electrons in the outer layer) sever as a doping element in the carbon (structured with 4 electrons in the outer layer) matrix, altering the electric density of the neighbor carbons, which may result in a more active carbon material. (Wei, 2015)

5.2.4.2 Catalyst effects texture of the N-CS

In order to understand how the catalyst concentration effects the texture of the carbon spheres, samples prepared with various catalyst concentration were tested by nitrogen adsorption/desorption.

Table 13 BET results of N-doped CS with various catalyst concentration

	Surface area _{BET} (m ² /g)	Pore volume _{micro} (m ³ /g)	Pore volume _{tot} (m ³ /g)	Sphere size (nm)
N_R/C_6_C750	507.1	0.231	0.264	800
N_R/C_1.2_C750	505.5	0.221	0.291	300
N_R/C_0.75_C750	530.4	0.230	0.342	170
N_R/C_0.5_C750	563.7	0.227	0.599	90
N_R/C_0.375_C750	642.0	0.253	0.834	60

This section is conducted to study the how the catalyst concentration influences the structure of the carbon spheres. Samples N_R/C_6_C750, N_R/C_1.2_C750 and N_R/C_0.75_C750 almost share the similar result in a 500 m²/g surface area and 0.3 m³/g total pore volume range. Surprisingly, the total pore volume shows a significant increase for the N_R/C_0.5_C750 and N_R/C_0.375_C750 samples, while the micro pore volume does not show theatrical increase. This indicates the development of mesoporosity and/or macroporosity. This also confirmed by the BET isotherm of sample N_R/C_0.5_C750 and N_R/C_0.375_C750. According to Figure 23, Carbon sphere N_R/C_0.375_C750 shows a IV type isotherm, which indicates development of mesoporosity.

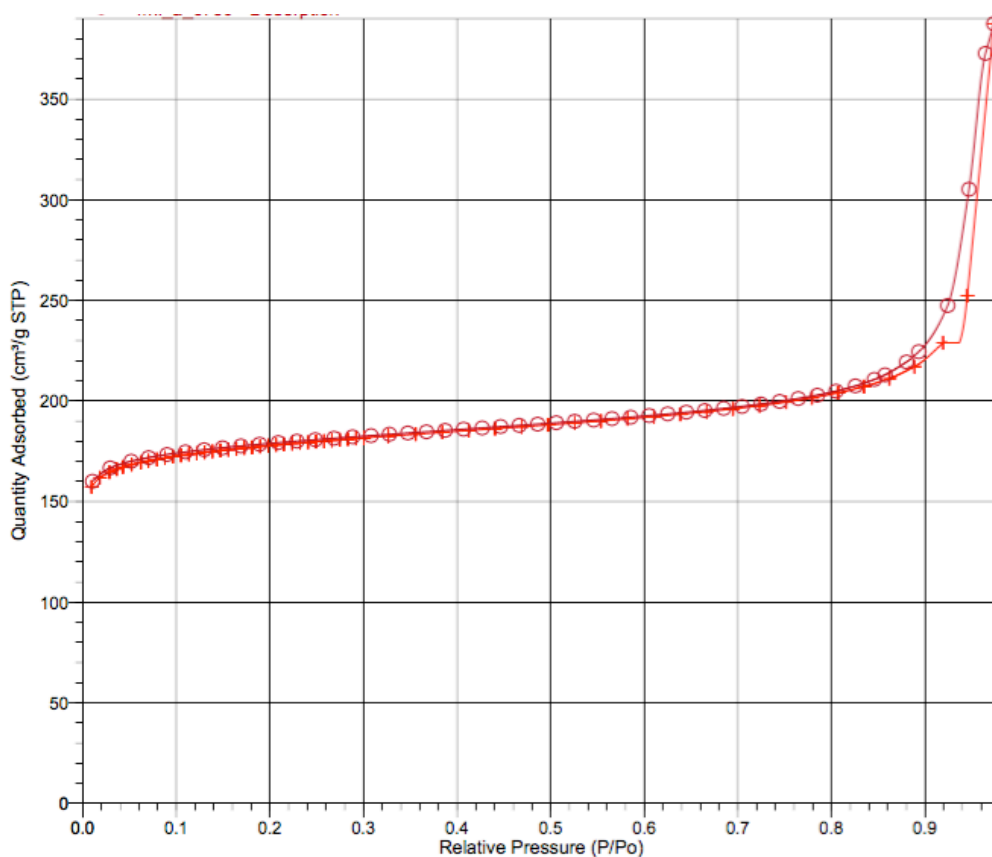


Figure 23 BET isotherm for N_R/C_0.375_C750

The mesoporosity of the N_R/C_0.5_C750 and N_R/C_0.375_C750 samples may be caused by the external gap among the nano-carbon spheres since the CS prepared with high catalyst concentration has a nano-scale structure (90nm for N_R/C_0.5_C750, 60nm for N_R/C_0.375_C750). In brief, there is no obvious evidence that has been found to support the connection between the catalyst concentration and the porosity, surface area of the spheres.

5.2.5 Activation of N-CS with phosphoric acid (H₃PO₄)

Only two samples were studied for phosphoric acid activation due to the poor results we obtained from nitrogen adsorption/desorption. The sample information is listed in Table 14.

Table 14 sample information of N-doped CS with H₃PO₄ activation

	HCHO (ml)	Resorcinol (g)	Melamine (g)	NH ₄ OH (ml)	Carbonization T(°C)	Activation T (°C)	Activation temperature (°C)	Carbonization T (°C)
N_RF_C600_A700	1	0.50	0.57	0.75	600	700	600	
N_RF_C750_A900	1	0.50	0.57	0.75	750	900	750	

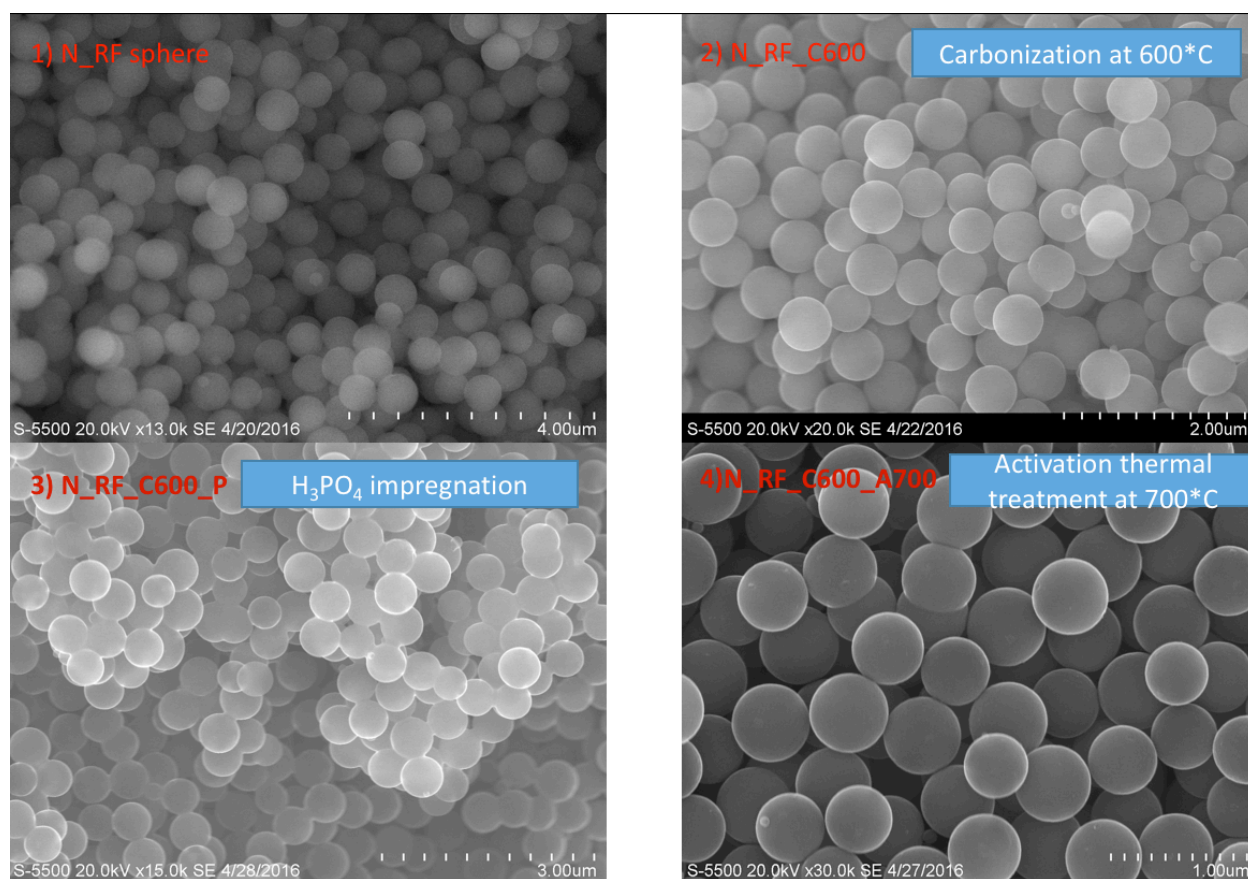


Figure 24 SEM image of N-doped CS 1) polymer spheres 2) after carbonization 3) after H₃PO₄ impregnation 4) after activation

Table 15 BET results of N-doped CS with H₃PO₄ activation

	Surface area _{BET} (m ² /g)	Pore volume _{micro} (m ³ /g)	Pore volume _{tot} (m ³ /g)
N_RF_C600	458.8	0.211	0.237
N_RF_C750	579.9	0.261	0.304
N_RF_C600_A700	329.5	0.113	0.139
N_RF_C750_A900	341.6	0.149	0.183

Figure 24 showing the morphology changes of the spheres during the phosphoric acid activation process. 1) The N-doped RF spheres; 2) N-doped RF spheres after carbonization at 600°C; 3) previous spheres after impregnation of phosphoric acid; 4) Final step, after activation thermal treatment at 700°C. According to Figure 24, the spherical shape has been perfectly maintained during the whole process. Image 3, after impregnation with phosphoric acid, the spheres start to merge with each other, which is often observed for phosphoric acid impregnation. Nevertheless, smooth surface is retained in the end showed in image 4 after thermal treatment. The BET surface area and pore volume in Table 15, not only have not been improved but drastically decreased for both samples. The reason may be the weak acidity of phosphoric acid and the highly ordered carbon-nitrogen structure after carbonization, make it difficult to break or defect the structure inside the carbon spheres.

5.2.6 Yielding

The weight after carbonization of the spheres has been recorded and listed below. Detailed calculations are showed in Appendix.

Table 16 yielding of N-doped CS

	Weight(mg)	yielding
RF_C600	308.6	38.5%
RF_C750	331.2	41.3%
RF_C900	280.8	34.9%
N_RF_C600	357.2	44.5%
N_RF_C750	327.5	40.8%
N_RF_C900	263.6	32.9%

Yields has been calculated with the assumption that spheres after carbonization are only composed with carbon. Detailed calculations are listed in the appendix.

5.2.7 Sum up N-CS

To the best our knowledge, this is the first time N-doped spheres are successfully synthesized using sonication method, simply by mixing melamine directly with resorcinol and formaldehyde into the solution. Furthermore, size tuning (from 50nm to 1000nm range) of the N-doped spheres is achieved by controlling the catalyst (ammonia aqueous solution) concentration. Moreover, N-CS are successfully synthesized by organic component (ethanol) free solvent. Modified N-CS, with a highest BET specific surface area and pore volume of 579.9m²/g and 0.304m³/g, respectively (before activation), do show increase of the surface area and pore volume compared with carbon spheres without nitrogen doping. The catalyst concentration does not have distinct effect on the surface area and pore volume of the N-doped CS. The activation of N-CS using phosphoric impregnation approach failed due to the weak interaction between the and H₃PO₄the carbon network.

5.3 Result of Si-template modified CS

To best our knowledge, this was the first time silica nanoparticles are successfully inserted homogeneously into the carbon spheres using an ultra-sonication method. As mentioned before, the carbonization process of the RF resin creates a certain amount of micropores (less than 2nm) caused by the escaping of small molecule like oxygen and hydrogen from the carbon matrix due to the high-temperature treatment. The silica template method is usually used to create more porosity, especially mesoporosity(2-50nm) to maximize the application of the spheres. Sample information is listed in Table 17

Table 17 sample information of Si-template modified CS

	HCHO (ml)	Resorcinol (g)	Silica (ml)	Water (ml)	EtOH (ml)	NH₄OH (ml)	Initial T(°C)	Power %	Carbonization T (°C)
Si_C600	1	1	0.65	100	40	0.75	25	30	600
Si_C750	1	1	0.65	100	40	0.75	25	30	750

5.3.1 SEM

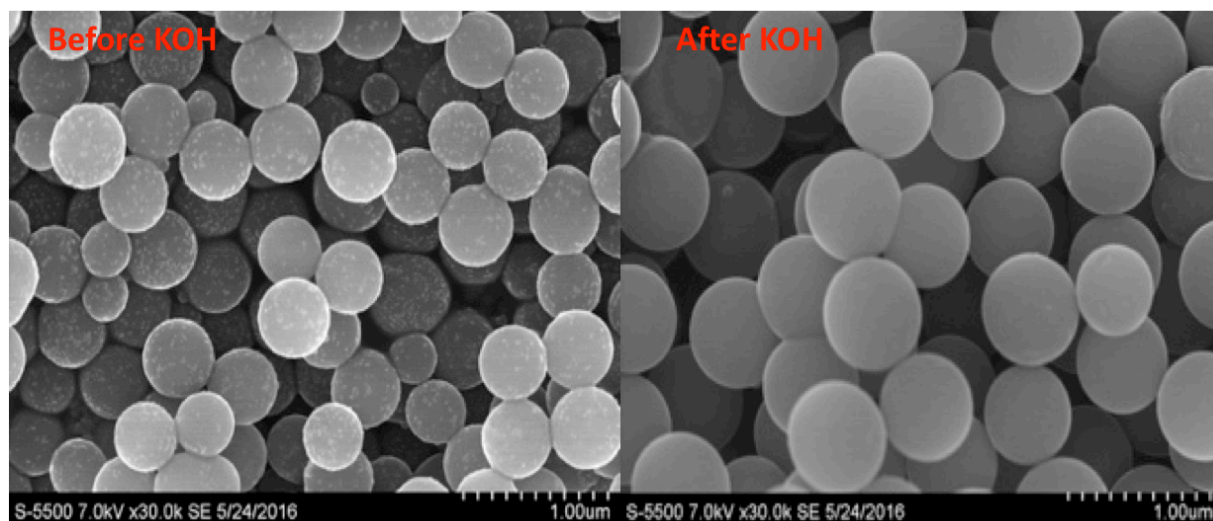


Figure 25 SEM image of Si-template CS (left) before KOH etch (right) after KOH etch

Figure 25 shows the morphology of the Si-RF spheres in each state: after polymerization, after carbonization at 750°C, after silica template has been removed by KOH solution. The spherical shape has been well maintained during each process. Interestingly, we can clearly observe homogeneously dispersed silica dots all over the spheres in the SEM image “after carbonization”. Moreover, the homogeneous dispersed brighter dots disappeared in the image “Si template removed”. These image indicates that silica nanoparticles have been successfully homogeneously inserted in the RF matrix and further successfully removed by using KOH solution.

5.3.2 EDS

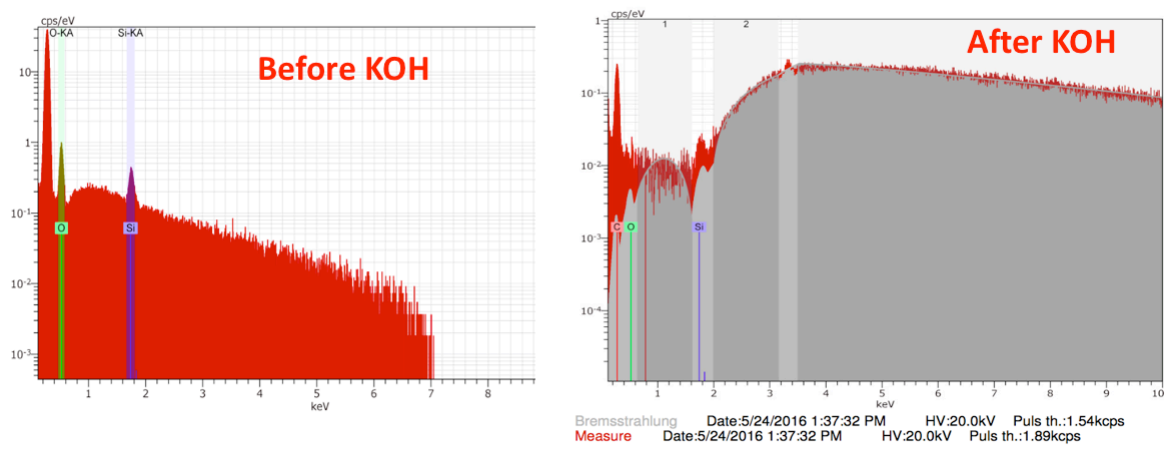


Figure 26 EDS spectra of Si-template CS (left) before KOH etch (right) after KOH etch

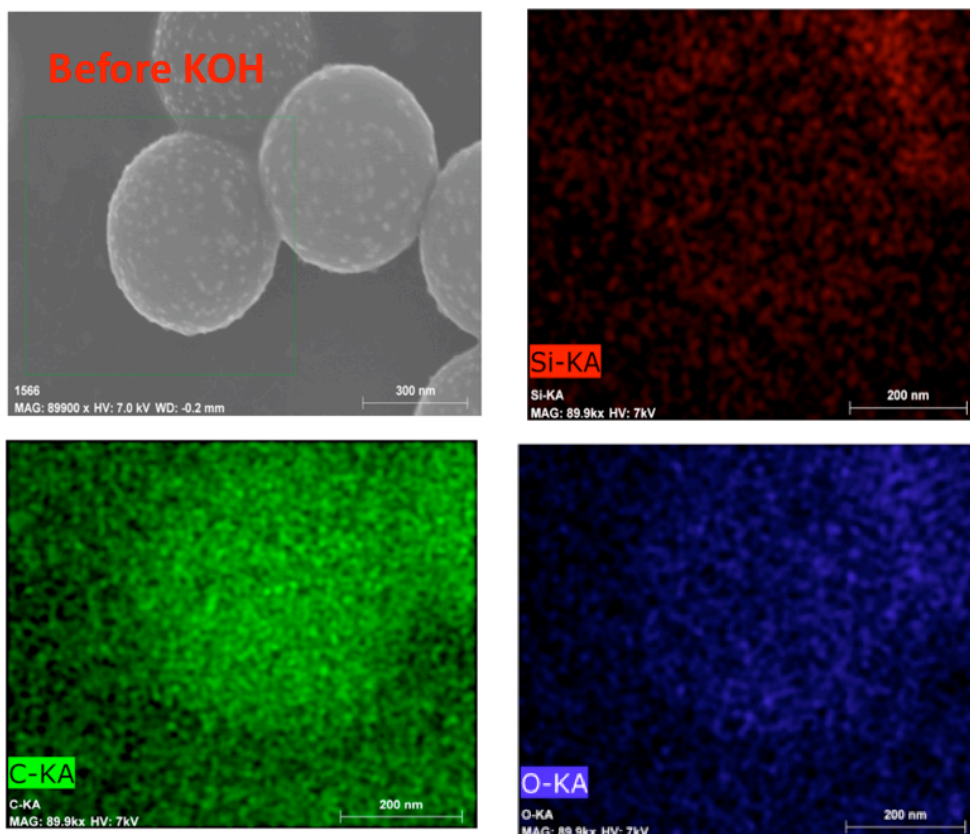


Figure 27 EDS mapping of Si-template CS before KOH etch

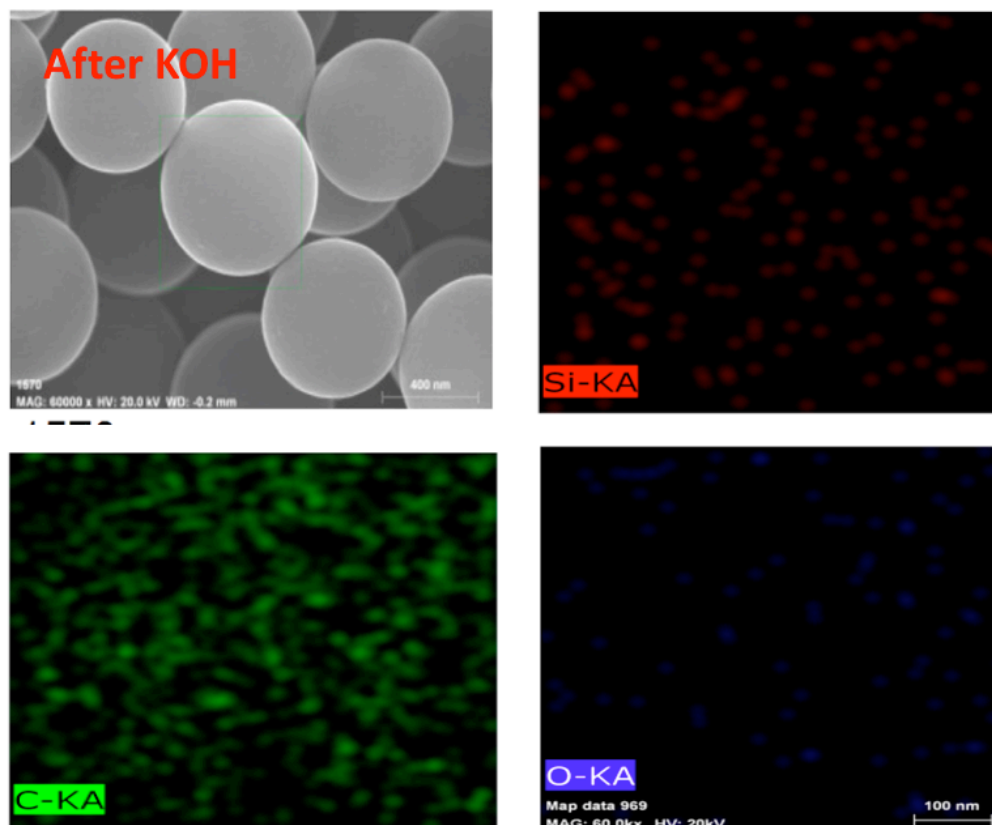


Figure 28 EDS mapping of Si-template CS after KOH etch

To ensure above conclusion, EDS had been conducted to trace the silica nanoparticles. The spectrum of the “before Si-removing” sample shows distinctive peaks at Si element and O element, while the “after Si-removing” spectrum shows no distinctive peaks at neither Si element nor O element. In addition, the EDS mapping gives the similar analysis showed in the Figure27 and Figure 28.

5.3.3 Structure properties(nitrogen adsorption/desorption) of Si-template Carbon spheres

The Table 18 shows BET specific surface area and pore volume of Si-template inserted carbon spheres. Sample carbonized at 600 °C and 750 °C before KOH etching denoted as Si_C600 and Si_C750, respectively. While sample carbonized at 600 °C and 750 °C after KOH etching denoted as Si_C600_KOH and Si_C750_KOH, respectively.

Table 18 BET results of Si-template modified CS

	Surface area _{BET} (m ² /g)	Pore volume _{micro} (m ³ /g)	Pore volume _{tot} (m ³ /g)
Si_C600	410.7	0.186	0.215
Si_C600_KOH	503.1	0.219	0.266
Si_C750	514.2	0.231	0.283
Si_C750_KOH	561.3	0.252	0.297

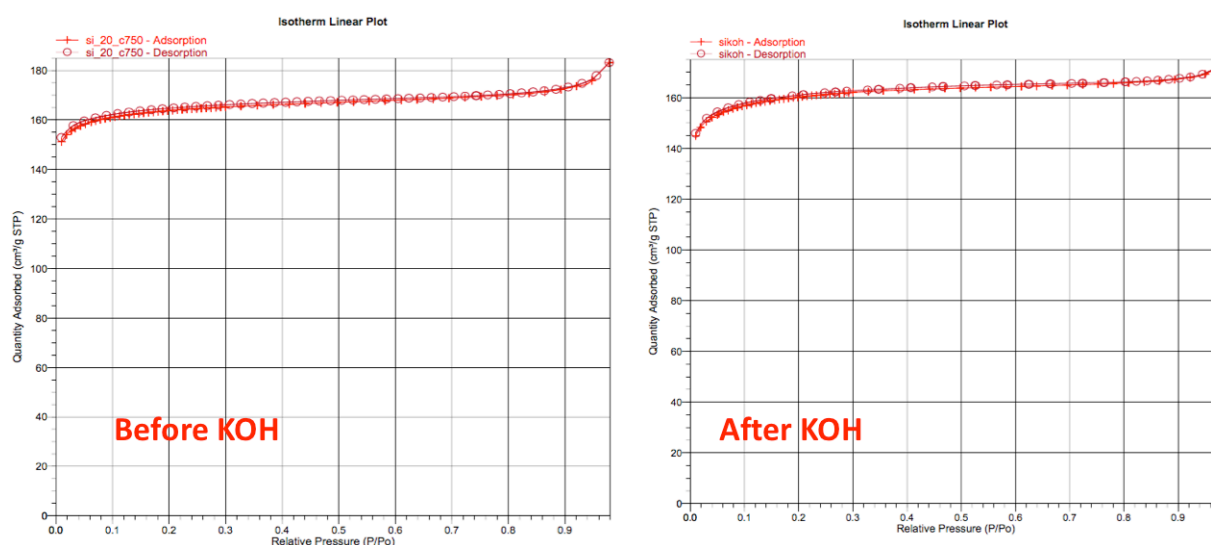


Figure 29 BET isotherm of Si-template CS before KOH etch

Surface area and pore volume are both increased after Si-template removing process for all samples. However, the increased pore volume was not coming from mesopores, as we expected, but still from micropores. To further study the pore development of the sample, nitrogen adsorption and desorption isotherm has been investigated here.

The nitrogen adsorption/desorption isotherm of both “Si-RF sphere after carbonization” and “Si-RF spheres after SiO₂ removed” are of type I recommended by the IUPAC classification, indicating the development of microporous structure in the samples. The expected type IV isotherm, typical isotherm for mesoporous materials, was not be presented in sample “Si-RF spheres after SiO₂ removed”, which indicates the failure of creating noticeable amount of mesoporosity by using the Si-template method.

6 CONCLUSION

The rapid synthesis (within five minutes) of monodispersed CS, N-CS and silica-template modified CS are consistently maintained with an ultrasonic method.

Optimizing R/F molar ratio, solvent composition and temperature gradient are the key parameters to generate uniform spherical spheres. Lower sonication power reduces the aggregation of the spheres. Specific optimized parameters in this work are listed here: R/F molar ratio, water to total solvent percentage and the sonication power are set to be 7:8, 70v% and 30%, respectively, in room temperature(25°C).

N-doped carbon particle size tuning, from nano-range to submicro-range (40nm to 1000nm range), is achieved by varying the catalyst concentration in the solution. In general, the diameter of the N-CS decreases with increasing the concentration of the catalyst. It is worthy mentioning that, the N-CS were also successfully synthesized without any organic solvent (ethanol). The activation of N-CS using phosphoric impregnation approach failed due to the weak interaction between the H_3PO_4 and the carbon network.

The porosity of the carbon spheres has been enhanced by sacrificing silica template. However, the improvement is still far away from what we expected, especially in the mesoporous domain.

The CS, N-CS and Si-template modified CS (carbonized at 750 °C) are classified as microporous materials with a highest BET specific surface area of 502.8m²/g, 642.0m²/g and 561.3m²/g, respectively; highest pore volume of 0.260m³/g, 0.834m³/g and 0.297m³/g respectively, before activation.

7 FUTURE WORK

In order to have a better understanding of the effect of nitrogen doping on the CS, the quantitatively analysis of nitrogen uptake and nitrogen composition of N-CS should be conducted with X-ray photoelectron spectroscopy (XPS).

The activation of CS/N-CS via H_3PO_4 failed in this work. However, some other activation method can also be tested in the future work, such as KOH activation, CO_2 activation and etc.

Using additional specific surfactants may be a solution to control the silica template size, thus the porous size inside the CS introduced by hard template method.

Some applications (such as catalyst support, drug delivery and etc.) of the produced CS/N-CS can also be tested in the future work

BIBLIOGRAPHY

- [1] Alazemi, A. A. (2015). Ultrasooth Submicrometer Carbon Spheres as Lubricant Additives for Friction and Wear Reduction. *Applied materials & interfaces* , 5514-5521.
- [2] Al-Muhtaseb, S. (2003). Preparation and Properties of Resorcinol–Formaldehyde Organic and Carbon Gels. *Advanced Material*, 15 (2), 101-114.
- [3] Bazargan, A. (2013). A Review: Synthesis of Carbon-Based Nano and Micro Materials by High Temperature and High Pressure. *American Chemical Society*, 52 (36), 12689-12702.
- [4] Blaha, M. (2013). Effects of the polymerization temperature on the structure, morphology and conductivity of polyaniline prepared with ammonium peroxodisulfate. *European Polymer Journal*, 49 (12), 3904-3911.
- [5] Deshmukh, A. A. (2010). Carbon spheres. *Materials Science and Engineering R* , 1 (28), 1-28.
- [6] Elkhatat, A. (2011). Advances in Tailoring Resorcinol-Formaldehyde Organic and Carbon Gels. *Advanced Materials*, 23 (26), 2887–2903.
- [7] Ewert, J.-K. (2015). Enhanced capacitance of nitrogen-doped hierarchically porous carbide-derived carbon in matched ionic liquids. *The Royal Society of Chemistry* , 3, 18906-18912.
- [8] Ferrero, G. A. (2016). The influence of pore size distribution on the oxygen reduction reaction performance in nitrogen doped carbon microspheres. *Journal of Materials Chemistry A*, 4, 2581.
- [9] Goldstein, J. (1992). *Scanning Electron Microscopy and X-ray Microanalysis*. new york: plenum press.
- [10] Horikawa, T. (2004). Size control and characterization of spherical carbon aerogel particles from resorcinol–formaldehyde resin. *carbon* , 169-175.
- [11] Kim, D.-S. (2004). Activated Carbon from Peach Stones Using Phosphoric Acid Activation at Medium Temperatures. *Journal of Environmental Science and Health* , 1301-1318.
- [12] Kinoshita, S., Yoshioka, S., & Miyazaki, J. (2008). Physics of structural colors. *Reports on Progress in Physics*, 71 (1), 76401.
- [13] Lee, J. (2004). Synthesis of new nanoporous carbon materials using nanostructured silica materials as templates. *Journal of Materials Chemistry* , 14, 478-486.

- [14] LI, R. (2015). A Review of Hydrothermal Carbonization of Carbohydrates for Carbon Spheres Preparation. *Trends in Renewable Energy - Journal*, 1 (1), 43-56.
- [15] Liu, J. (2013). A facile soft-template synthesis of mesoporous polymeric and carbonaceous nanospheres. *Nature Communications*, 4 (2798), 1-7.
- [16] Liu, X. (2014). From melamine-resorcinol-formaldehyde to nitrogen-doped carbon xerogels with micro- and meso-pores for lithium batteries. *Journal of Materials Chemistry A*, 2 (35), 14429-14438.
- [17] malvern. (2016, Jan 12). *Nanoparticle Tracking Analysis Visualize and measure particle size and concentration*. Retrieved April 10, 2016, from malvern:<http://www.malvern.com/en/products/technology/nanoparticle-tracking-analysis/>
- [18] McMullan, D. (1988). Von Ardenne and the scanning electron microscope. *royal microscopical society*, 23, 283-288.
- [19] Nilantha, P. (2014). Nitrogen Enriched Porous Carbon Spheres: Attractive Materials for Supercapacitor Electrodes and CO₂ Adsorption. *chemistry of materials*, 26 (9), 2820-2828.
- [20] olawale, A. S. (2011). Preparation of phosphoric acid activated carbons from Canarium Schweinfurthii Nutshell and its role in methylene blue adsorption. *Journal of Chemical Engineering and Materials Science*, 6 (2), 9-14.
- [21] Peer, M. (2013). On the effects of emulsion polymerization of furfuryl alcohol on the formation of carbon spheres and other structures derived by pyrolysis of polyfurfuryl alcohol. *Carbon*, 51, 85-93.
- [22] Qi, Y. (2016). Mechanism for the formation and growth of carbonaceous spheres from sucrose by hydrothermal carbonization. *RSC Advanced*, 6, 20814.
- [23] Sharma, C. (2009). Synthesis of carbon xerogel particles and fractal-like structures. *Chemical Engineering Science*, 64 (7), 1536-1543.
- [24] Stöber, W. (1968). Controlled Growth of Monodisperse Silica Spheres in the Micron Size Range. *colloid interface science* , 62-69.
- [25] Stejskal, J. (1998). The effect of polymerization temperature on molecular weight, crystallinity, and electrical conductivity of polyaniline. *Synthetic Metals*, 96 (1), 55-61.
- [26] Sun, J. (2013). Structural coloration in nature. *RSC advanced* , 14862-14889.
- [27] Tang, j. (2015). Synthesis of Nitrogen-Doped Mesoporous Carbon Spheres with Extra-Large Pores through Assembly of Diblock Copolymer Micelles. *Angewandte Chemie International Edition*, 54 (2), 588-593.

-
- [28] Venugopal, V. (2015). Nano Focus: Structural details elicit color variety in photonic balls . *Materials Research Society* .
- [29] Vilas, G. (2014). Tunable, Functional Carbon Spheres Derived from Rapid Synthesis of Resorcinol-Formaldehyde Resins. *APPLIED MATERIALS & INTERFACES*, 6 (13), 10649–10655.
- [30] Wang, j. (2012). KOH activation of carbon-based materials for energy storage. *Journal of Materials Chemistry*, 22, 23710-23725.
- [31] webb, P. (2002). *Analytical Methods in Fine Particle Technology*. oxford: oxford university press.
- [32] Wei, Q. (2015). Nitrogen-Doped Carbon Nanotube and Graphene Materials for Oxygen Reduction Reactions. *Catalysts*, 5 (3), 1574-1602.
- [33] Wickramaratne, N. P. (2014). Nitrogen Enriched Porous Carbon Spheres: Attractive Materials for Supercapacitor Electrodes and CO₂ Adsorption. *chemistry of materials*, 26 (9), 2820–2828.
- [34] Xia, Y. (2000). Monodispersed Colloidal Spheres: Old Materials with New Applications. *Advanced materials*, 12 (10), 693–713.
- [35] Yakout, S. (2011). Characterization of activated carbon prepared by phosphoric acid activation of olive stones. *Arabian Journal of Chemistry*, 2 (9), 1489-1495.
- [36] Yang, T. (2014). N-doped mesoporous carbon spheres as the oxygen reduction reaction catalysts. *journal of materials chemistry A*, 2, 18139-18147.
- [37] Zhang, L. (2012). Nitrogen doping of graphene and its effect on quantum capacitance, and a new insight on the enhanced capacitance of N-doped carbon. *Energy & Environmental Science*, 5, 9618-9625.

APPENDIX A. CALCULATION OF SAMPLE COMPOSITION RATIOS

Water to total solvent (water and ethanol) volumetric ratio

$$W/T = \frac{\text{volume of water(ml)}}{\text{volume of water (ml) + volume of ethanol(ml)}} * 100\%$$

Table 19 water to total solvent volumetric ratio in different samples

W/E	RF_W100%	RF_W70%	RF_W60%	RF_W50%
Water(ml)	140	100	85	70
Ethanol(ml)	0	40	55	70
W/Total Volume ratio	100%	70%	60%	50%

R/F molar ratio

Formaldehyde (37wt% in aqueous solution stabilized by 10% methanol,

$$m_F = v_F * \rho * 37\% = v_c * 1\text{g/ml} * 37\%$$

$$R/F = \frac{mR/110.1}{mF/30.03} * 100\%$$

Molar Mass of R=110.1g/mol

Molar Mass of F=30.03g/mol

Table 20 R/F molar ratio for different samples

	RF_R/F_1:2	RF_R/F_3:5	RF_R/F_7:8	RF_R/F_1:1
Formaldehyde (ml)	1.4	1.2	1	0.8
Resorcinol(g)	1	1	1	1
R/F molar ratio	1:2	3:5	7:8	1:1

R/C molar ratio.NH₄OH (25wt%)

$$m_c = v_c * \rho * 25\% = v_c * 0.9 \text{g/ml} * 25\%$$

$$R/C = \frac{mR/110.1}{mC/35.04} * 100\%$$

Molar Mass of NH₄OH=35.04g/mol*Table 21 R/C molar ratio for different samples*

	Resorcinol (g)	NH₄OH(ml)	R/C molar ratio
RF_R/C_6	0.5	0.25	6
RF_R/C_2	0.5	0.75	2
RF_R/C_1.2	0.5	1.25	1.2
RF_R/C_0.75	0.5	2	0.75
RF_R/C_0.5	0.5	3	0.5
RF_R/C_0.375	0.5	4	0.375
RF_R/C_0.3	0.5	5	0.3
RF_R/C_0.15	0.25	5	0.15

APPENDIX B. N-CS SIZE DATA FROM SEM AND NANOSIGHT

Sample information of N-CS is showed in Table 4

Table 22 sample information of N-CS prepared by various catalyst concentration

	HC HO (ml)	Reso rcin ol (g)	Mela mine (g)	Water (ml)	EtO H (ml)	NH₄O H (ml)	Initial T(°C)	Pow er %	Reactio n time (min)
N_R/C_6	1	0.50	0.57	100	40	0.25	25	30	5
N_R/C_2	1	0.50	0.57	100	40	0.75	25	30	5
N_R/C_1.2	1	0.50	0.57	100	40	1.25	25	30	5
N_R/C_0.75	1	0.50	0.57	100	40	2	25	30	5
N_R/C_0.5	1	0.50	0.57	100	40	3	25	30	5
N_R/C_0.375	1	0.50	0.57	100	40	4	25	30	5
N_R/C_0.3	1	0.50	0.57	100	40	5	25	30	5
N_R/C_0.15	1	0.25	0.28	100	40	5	25	30	5

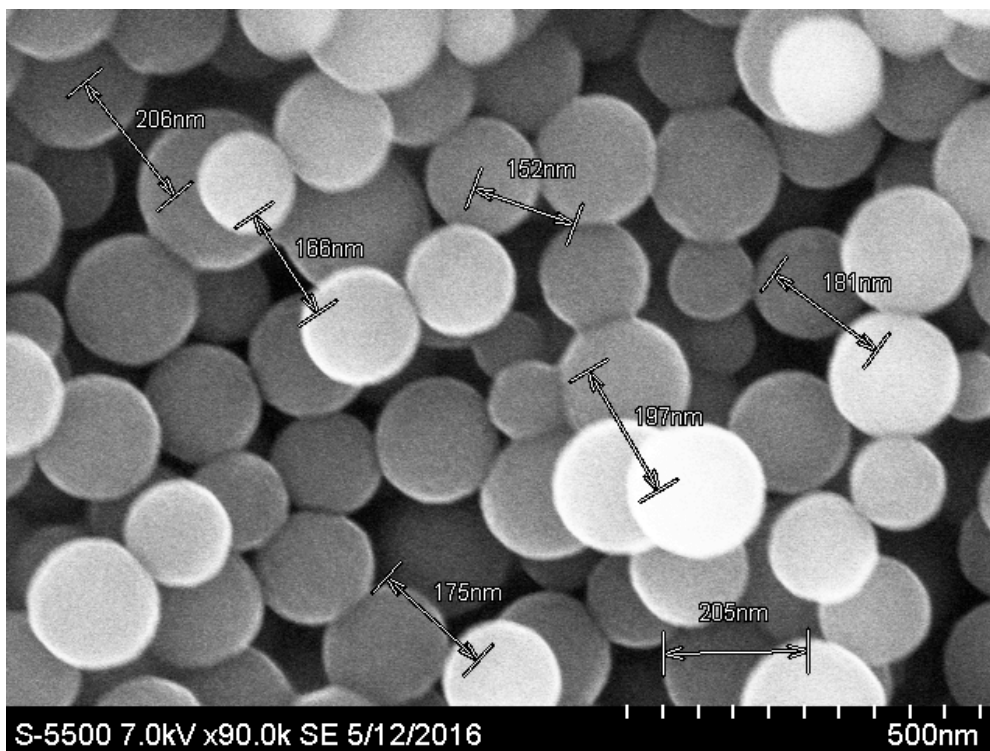


Figure 30 SEM image of *N_R/C_0.75* with marked scale

NANOSIGHT

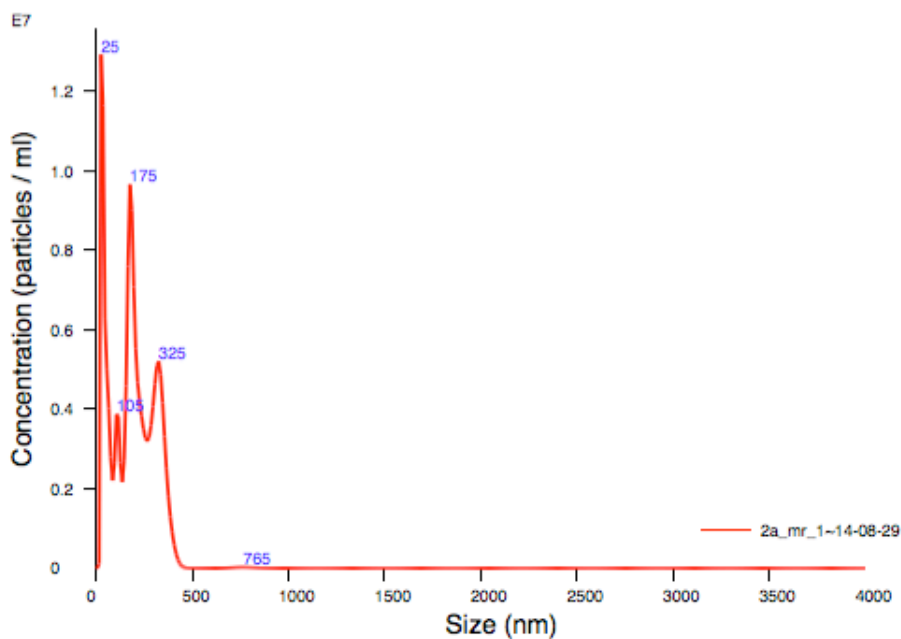


Figure 31 Size distribution from Nanosight of sample N_R/C_0.75

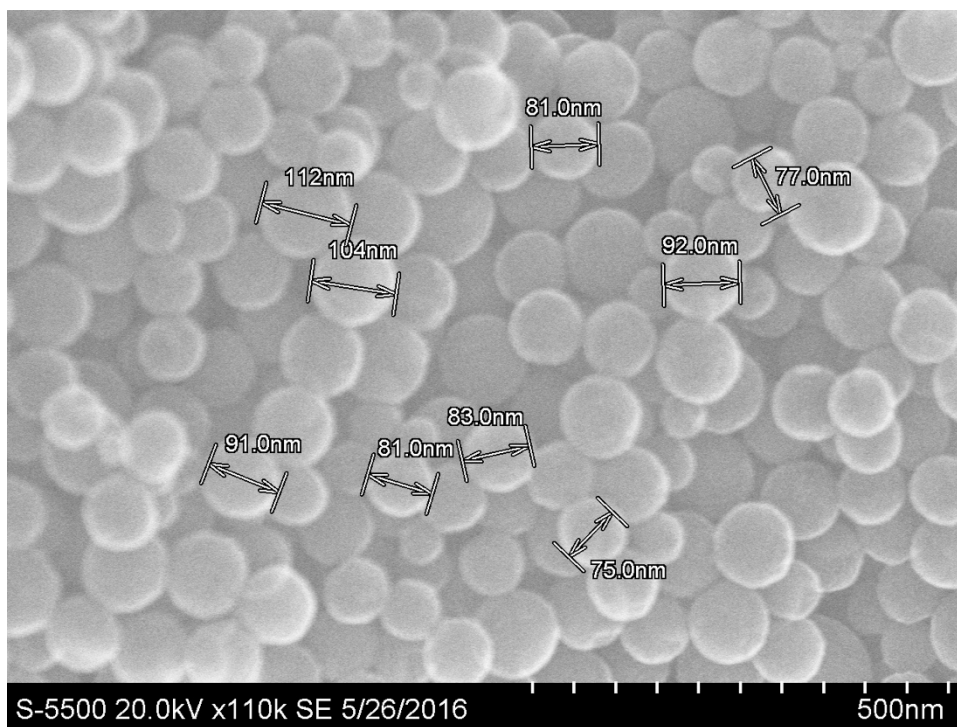


Figure 32 SEM image of N_R/C_0.5 with marked scale

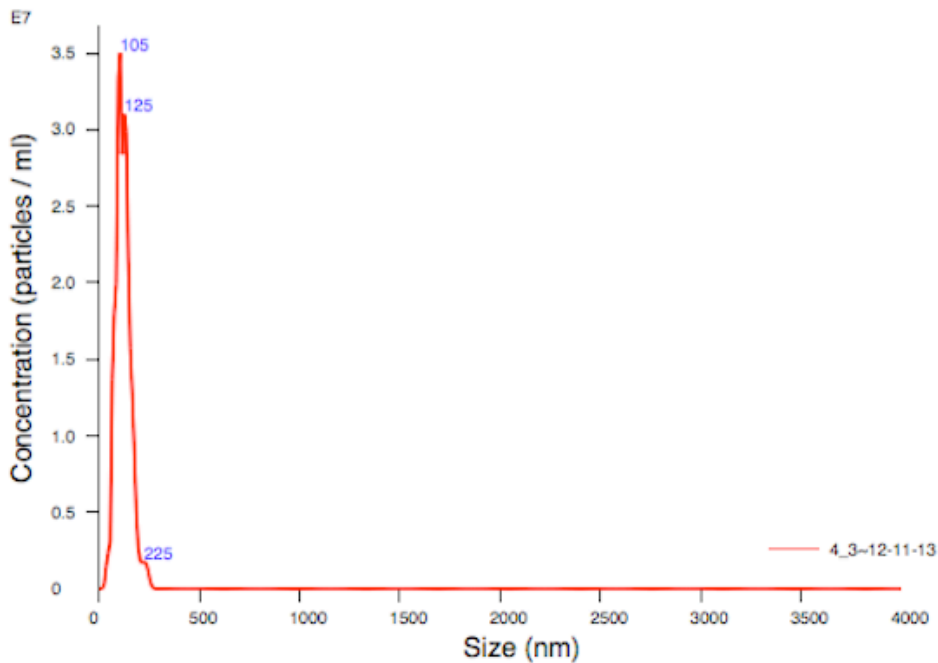


Figure 33 Size distribution from Nanosight of sample N_R/C_0.5

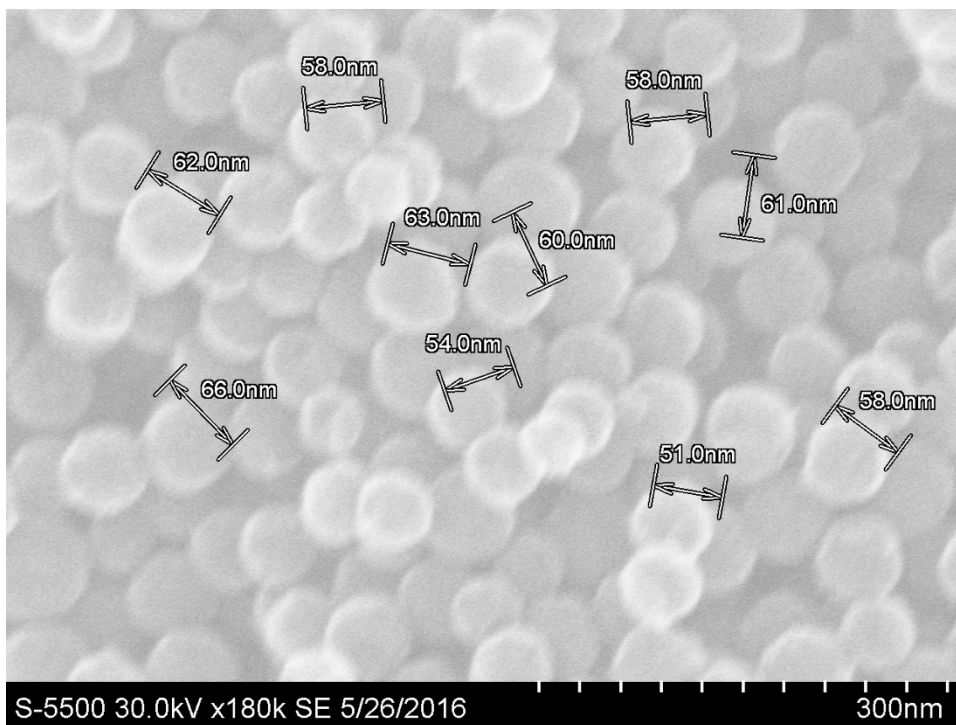


Figure 34 SEM image of N_R/C_0.375 with marked scale

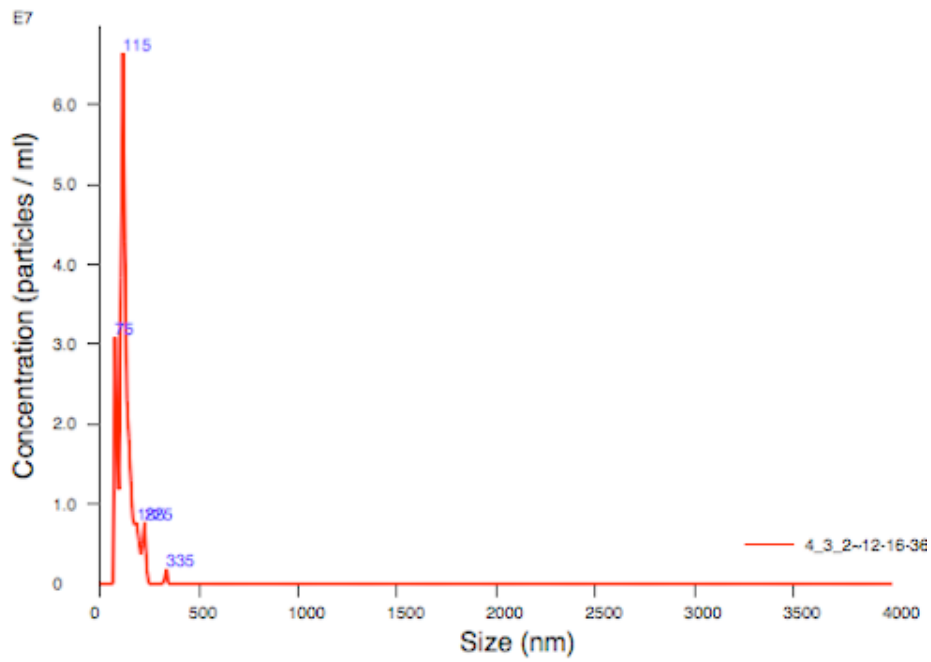


Figure 35 Size distribution from Nanosight of sample N_R/C_0.375

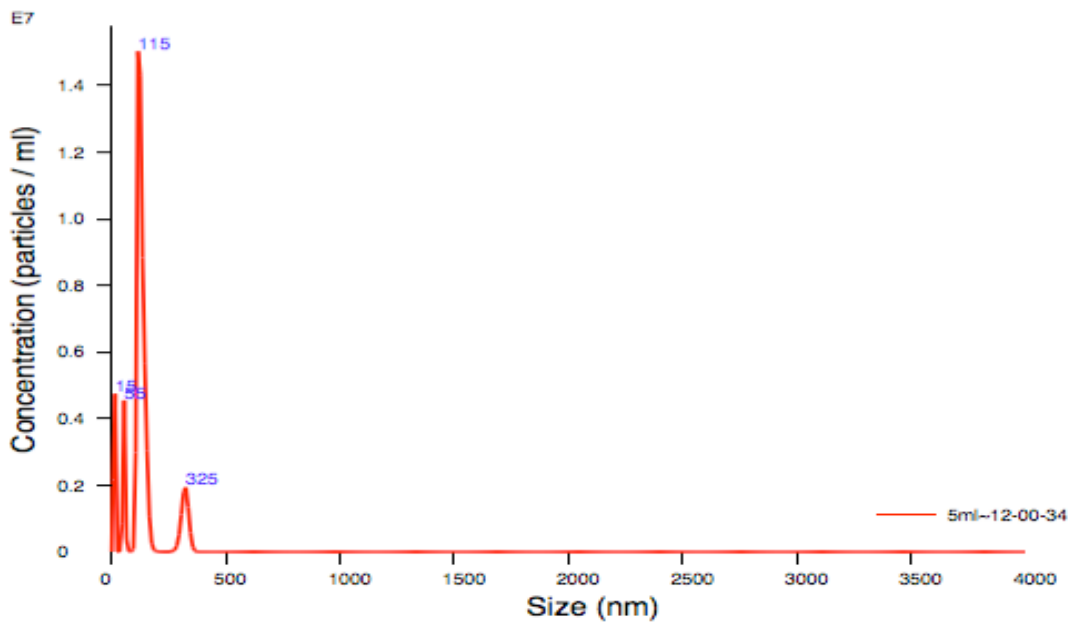


Figure 36 Size distribution from Nanosight of sample N_R/C_0.3

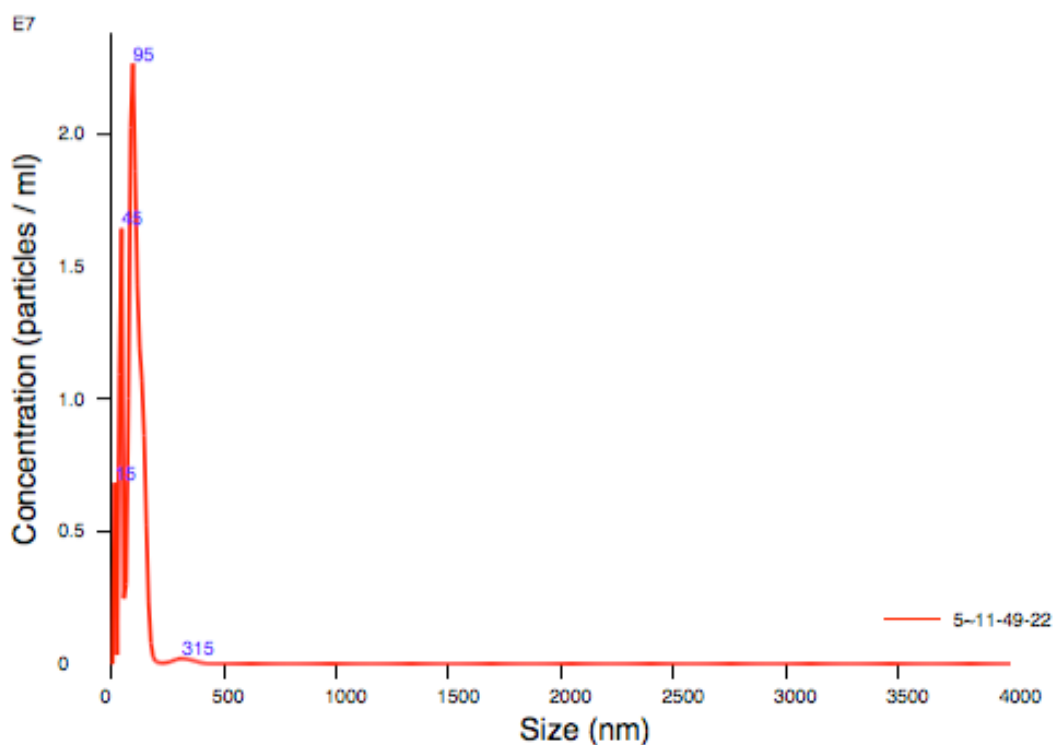


Figure 37 Size distribution from Nanosight of sample N_R/C_0.15

According to Figure 5, the spheres in the SEM image showed a size range from 50 nm to 60nm, However, the NTA showed a peak at 115 nm, which is as twice the size as what measured from SEM. We believe this doubled size collected from NTA may attribute to the cohesion of two spheres in the solution when conducting the NTA measurements. In the same manner, in Figure 4. There are peaks at 105 nm, 125 nm and 225nm, which the 225nm is about twice the size as 105 and 125nm. This “doubling size peaks” (the larger size peak is about twice the size as previous smaller peak) are also observed in the other samples in Figure 2, Figure 6, Figure 7 and Figure 8. Thus, we assign the smaller peak as individual sphere size.

APPENDIX C. ISOTHERM OF NITROGEN ADSORPTION/DESORPTION

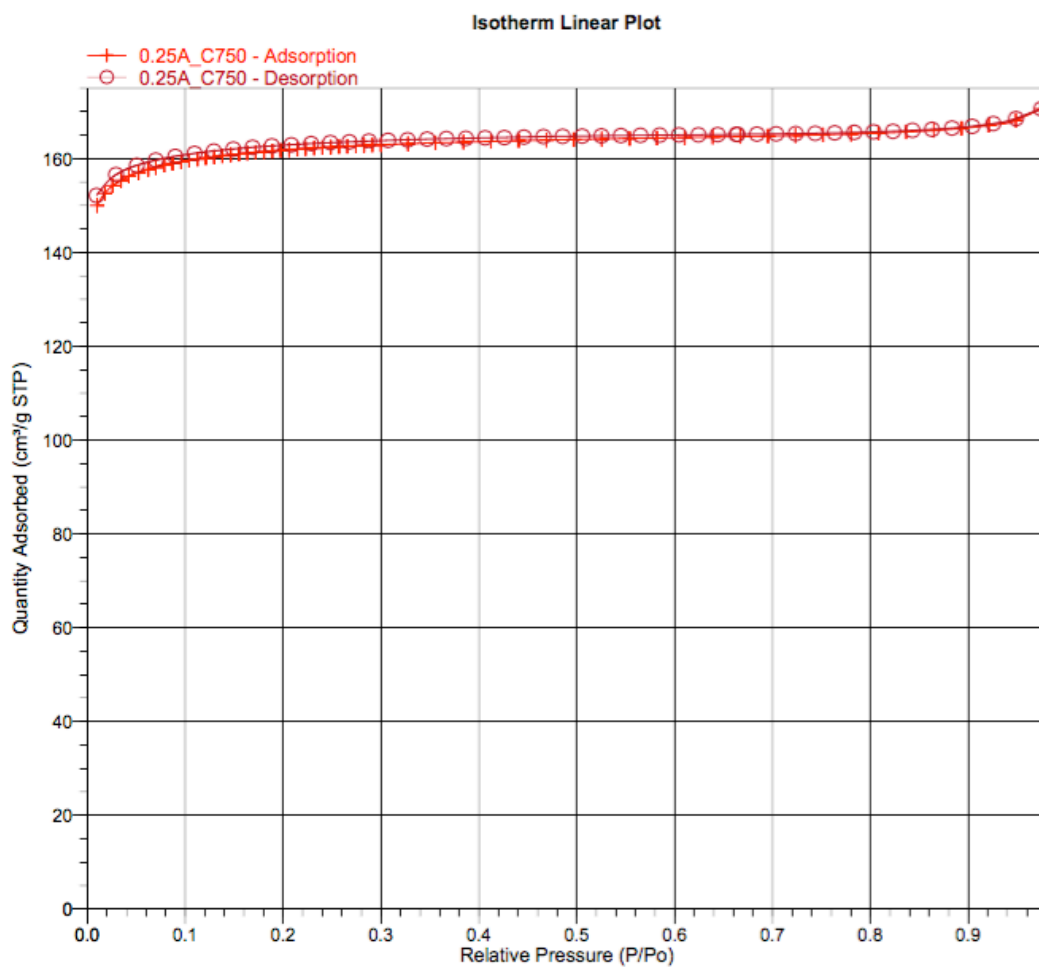


Figure 38 BET isotherm of sample N_R/C_6_C750

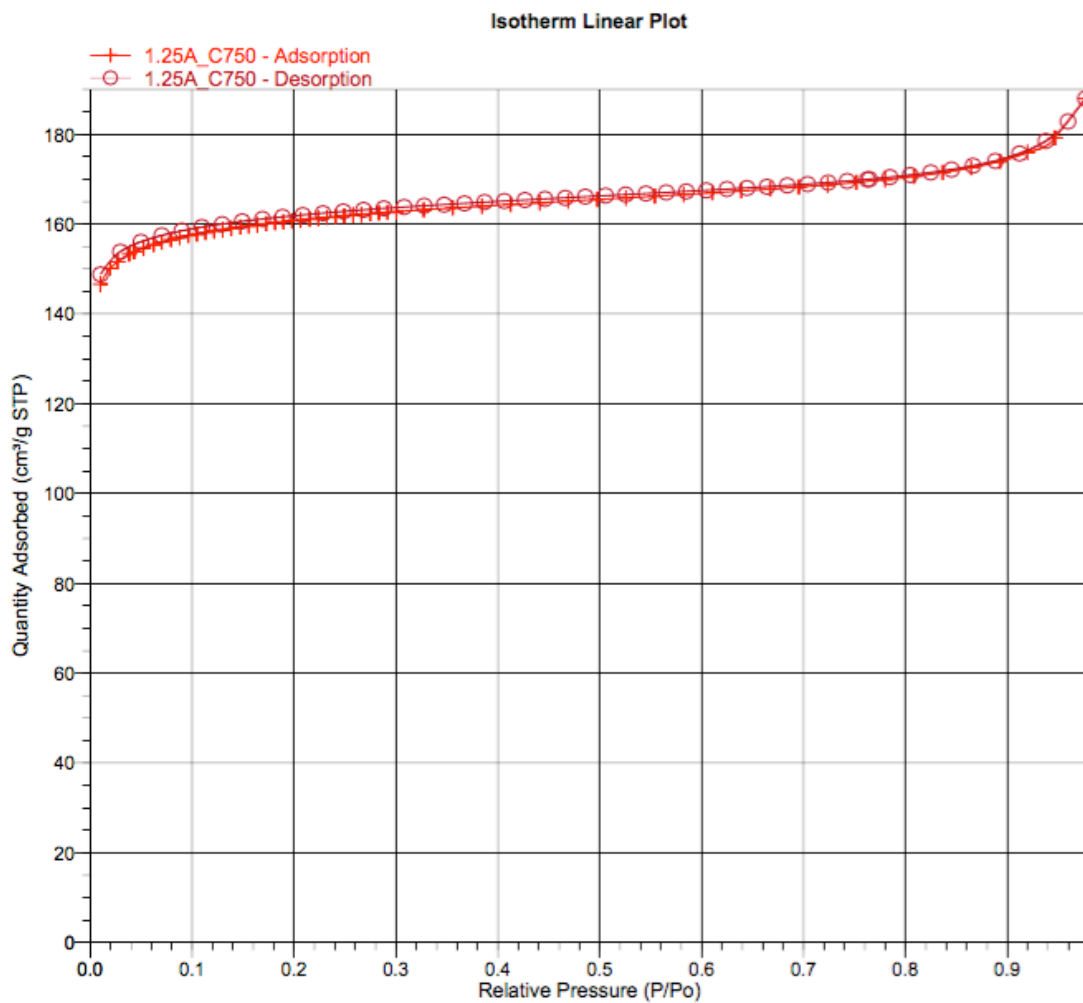


Figure 39 BET isotherm of sample N_R/C_1.2_C750

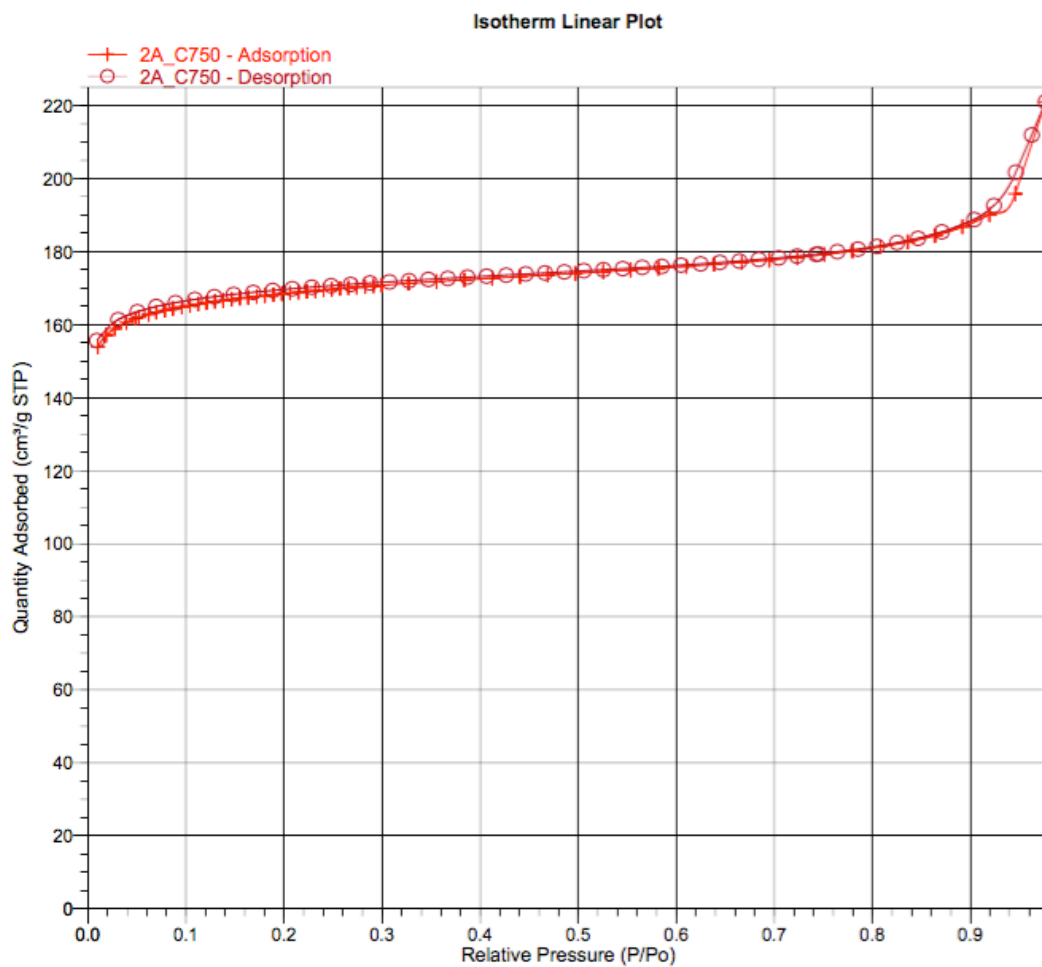


Figure 40 BET isotherm of sample N_R/C_0.75_C750

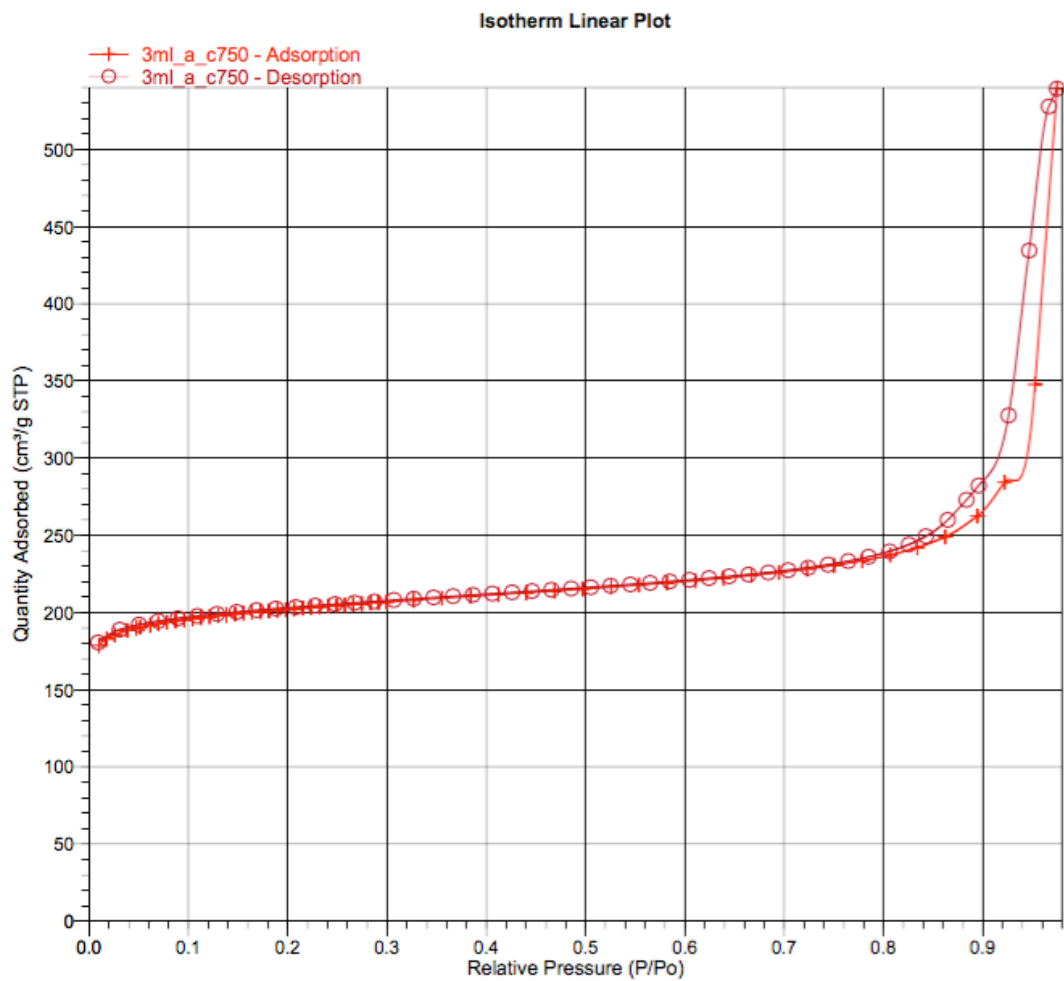


Figure 41 BET isotherm of sample N_R/C_0.5_C750

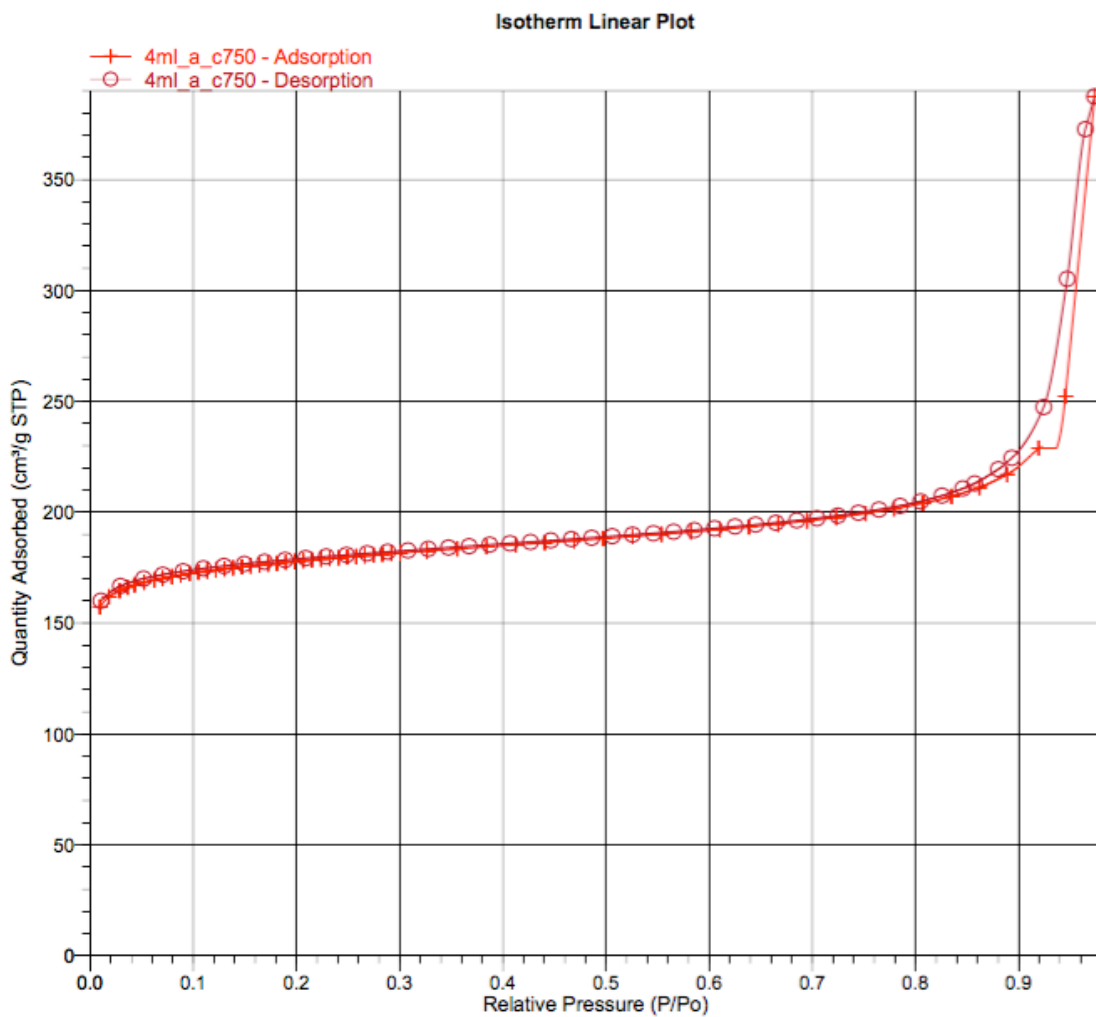


Figure 42 BET isotherm of sample N_R/C_0.375_C750

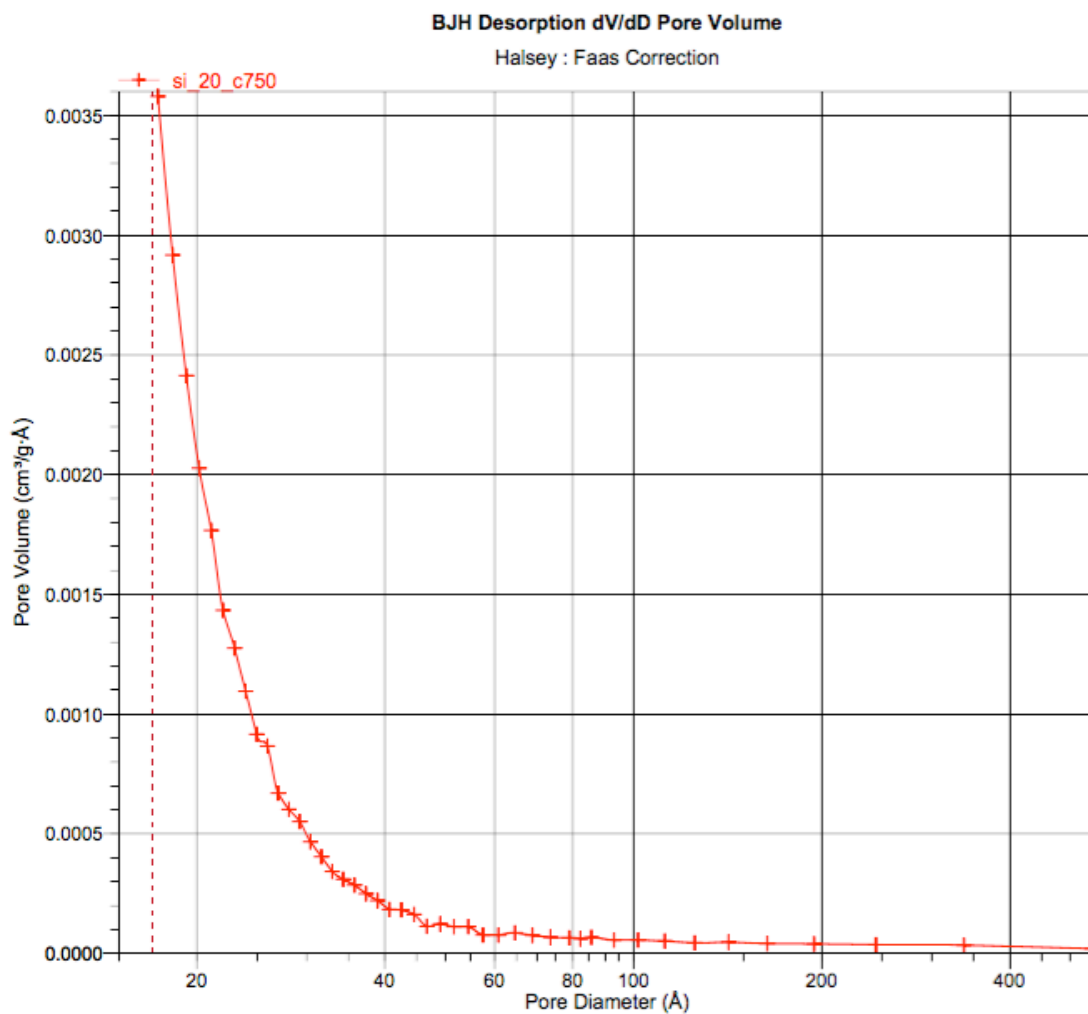


Figure 43 BJH Desorption dA/dD Pore Area analysis of Si_C750

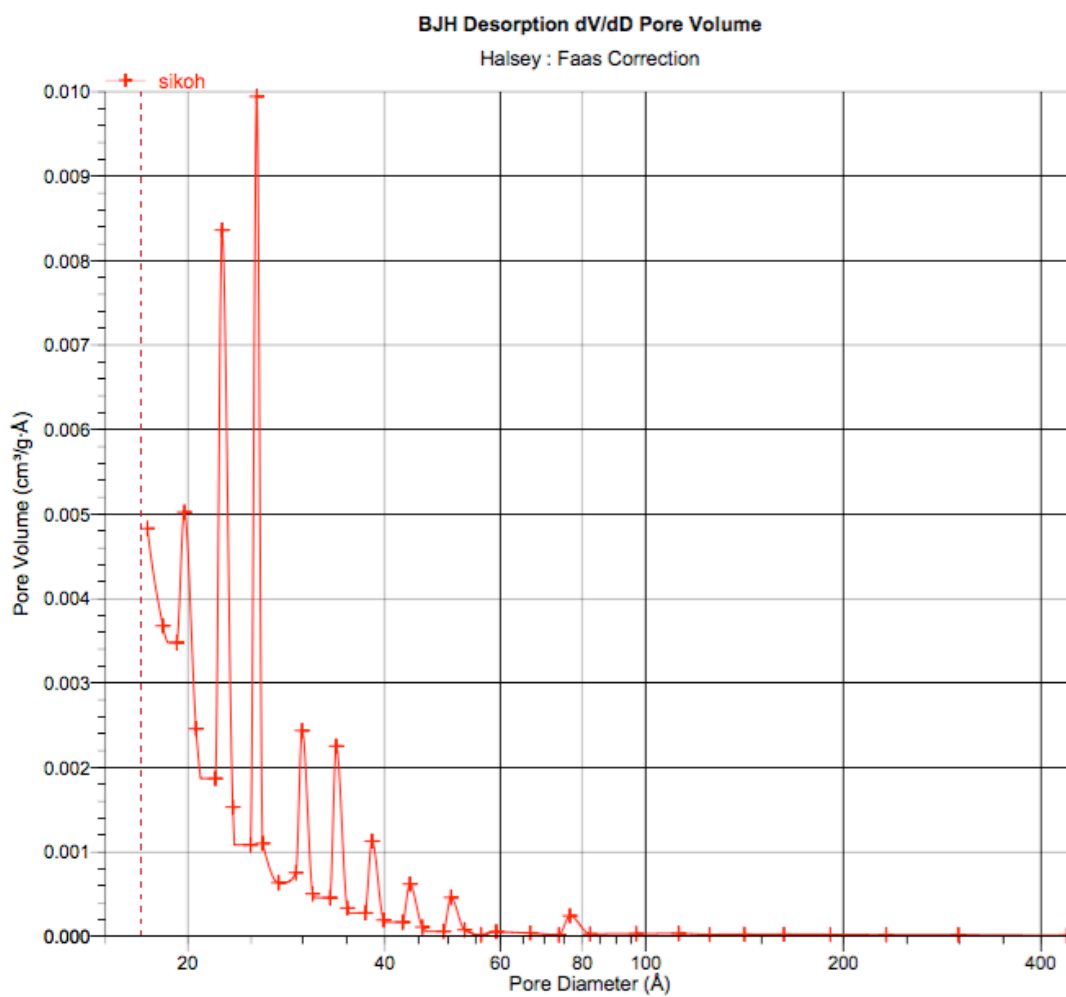


Figure 44 BJH Desorption dA/dD Pore Area analysis of Si_C750_KOH

APPENDIX D. N-DOPED SPHERES YIELDING CALCULATION

Carbon resource from resorcinol($C_6H_6O_2$)

$$1(\text{g}) * 12.01 * 6 / 110.11 = 0.6544(\text{g})$$

Carbon resource from formaldehyde(CH_2O)

$$1(\text{ml}) * 1(\text{g/ml}) * 37\text{wt}\% * 12.01 / 30.03 = 0.148(\text{g})$$

In total: carbon feeding resource $0.6544 + 0.148 = 0.8024\text{g}$

APPENDIX E. HSE RISK ASSESSMENT

ID	1726	Status	Dato
Risikoområde	Risikovurdering: Helse, miljø og sikkerhet (HMS)	Opprettet	11.11.2015
Opprettet av	Cristian Ledesma Rodriguez		
Ansvarlig	Wei Ge	Tiltak besluttet	
		Avsluttet	

Master - Catalysis, 2015, Wei Ge

Gyldig i perioden:

8/31/2015 - 7/1/2016

Sted:

3 - Gløshaugen / 315 - Kjemi 5

Mål / hensikt

This risk assessment contains all the activities that the master student Wei Ge will perform in the labs of the Catalysis group.

Bakgrunn

- Furnace
- Hot oil bath
- Gas distribution system/cylinders

Beskrivelse og avgrensninger

Forutsetninger, antakelser og forenklinger

[Ingen registreringer]

Vedlegg

[Ingen registreringer]

Referanser

[Ingen registreringer]

Oppsummering, resultat og endelig vurdering

I oppsummeringen presenteres en oversikt over farer og uønskede hendelser, samt resultat for det enkelte konsekvensområdet.

Farekilde: Use of high temperature furnace



Uønsket Electric shock
hendelse:

Konsekvensområde:

Uønsket Uncontrolled heating
hendelse:

Konsekvensområde:

Helse

Risiko før  Risiko 
tiltak: etter
tiltak:

Uønsket Fire
hendelse:

Konsekvensområde:

Uønsket Burn damage
hendelse:

Konsekvensområde:

Farekilde: Use of compressed gases

Uønsket Uncontrolled expansion and depletion of O₂
hendelse:

Konsekvensområde:

Ytre miljø

Risiko før Risiko etter

tiltak: tiltak:

Uønsket Gas leakage
hendelse:

Konsekvensområde:

Farekilde: Use of chemicals as precursors

**Uønsket Spills on skin
hendelse:**

Konsekvensområde:

Farekilde: Preparation of pellets

**Uønsket Squeezing fingers
hendelse:**

Konsekvensområde:

Farekilde: Use of hot oil bath

Uønsket Burns
hendelse:

Konsekvensområde:

Farekilde: Use of acid and organic solutions

**Uønsket Spills on skin
hendelse:**

Konsekvensområde:

Endelig vurdering

Oversikt involverte enheter og personell

En risikovurdering kan gjelde for en, eller flere enheter i organisasjonen. Denne oversikten presenterer involverte enheter og personell for gjeldende risikovurdering.

Enhet /-er risikovurderingen omfatter

- Institutt for kjemisk prosessteknologi

Deltakere

Karin Wiggen Dragsten

Cristian Ledesma Rodriguez

De Chen

Lesere

[Ingen registreringer]

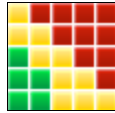
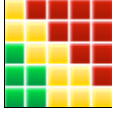
Andre involverte/interessenter

[Ingen registreringer]

**Følgende akseptkriterier er besluttet for risikoområdet
Risikovurdering: Helse, miljø og sikkerhet (HMS):**

Helse

**Materielle
verdier**



Oversikt over eksisterende, relevante tiltak som er hensyntatt i risikovurderingen

I tabellen under presenteres eksisterende tiltak som er hensyntatt ved vurdering av sannsynlighet og konsekvens for aktuelle uønskede hendelser.

Farekilde	Uønsket hendelse	Tiltak hensyntatt ved vurdering
Use of high temperature furnace	Electric shock	HSE documentation
	Electric shock	Working alone regulations at NTNU
	Electric shock	Personal protective equipment
	Uncontrolled heating	HSE documentation
	Uncontrolled heating	Working alone regulations at NTNU
	Uncontrolled heating	Personal protective equipment
	Fire	HSE documentation
	Fire	Working alone regulations at NTNU
	Fire	Personal protective

		equipment
	Fire	Ventilation
	Fire	Gas detectors
	Burn damage	HSE documentation
	Burn damage	Working alone regulations at NTNU
	Burn damage	Personal protective equipment
	Burn damage	Ventilation
Use of compressed gases	Uncontrolled expansion and depletion of O2	HSE documentation
	Uncontrolled expansion and depletion of O2	Working alone regulations at NTNU
	Uncontrolled expansion and depletion of O2	Personal protective equipment
	Uncontrolled expansion and depletion of O2	Ventilation
	Uncontrolled expansion and depletion of O2	Leak test procedure
	Uncontrolled expansion and depletion of O2	Installation and change of gas cylinders
	Gas leakage	HSE documentation
	Gas leakage	Working alone regulations

		at NTNU
	Gas leakage	Personal protective equipment
	Gas leakage	Ventilation
	Gas leakage	Leak test procedure
	Gas leakage	Installation and change of gas cylinders
Use of chemicals as precursors	Spills on skin	HSE documentation
	Spills on skin	Working alone regulations at NTNU
	Spills on skin	Personal protective equipment
Preparation of pellets	Squeezing fingers	HSE documentation
	Squeezing fingers	Working alone regulations at NTNU
	Squeezing fingers	Personal protective equipment
Use of hot oil bath	Burns	HSE documentation
	Burns	Working alone regulations at NTNU
	Burns	Personal protective equipment

Use of acid and organic solutions	Spills on skin	HSE documentation
	Spills on skin	Working alone regulations at NTNU
	Spills on skin	Personal protective equipment

Eksisterende og relevante tiltak med beskrivelse:

HSE documentation

The laboratories have an updated Room Card and the unit 2.4 has a copy of the risk assessment, operating instructions and apparatus card with information regarding safety and information in case of emergency stop. Different phone numbers are provided to contact in case of emergency.

Working alone regulations at NTNU

NTNU students and employee are not allowed to work alone after 7pm and during the weekends.

Working after 19:00 or in the weekends, you need to be at least 2 in the lab or in the building with regularly check-ups (every 30 minutes). Both of the people needs to have access to the labs

Ventilation

The reactor system is installed inside a cabinet with ventilation.

Gas detectors

The cabinet has CO/H₂ and CH₄/H₂ detectors which trigger the alarms in case of leakage. There are portable detectors that must be used during the leak tests before running experiments.

Leak test procedure

Before running experiments, a leak test must be performed following the procedure attached.

Installation and change of gas cylinders

This will be done by authorized personnel only.

Risikoanalyse med vurdering av sannsynlighet og konsekvens

I denne delen av rapporten presenteres detaljer dokumentasjon av de farer, uønskede hendelser og årsaker som er vurdert. Innledningsvis oppsummeres farer med tilhørende uønskede hendelser som er tatt med i vurderingen.

Følgende farer og uønskede hendelser er vurdert i denne risikovurderingen:

- **Use of high temperature furnace**

- Electric shock

- Uncontrolled heating

- Fire

- Burn damage

- **Use of compressed gases**
 - Uncontrolled expansion and depletion of O₂

 - Gas leakage

- **Use of chemicals as precursors**
 - Spills on skin

- **Preparation of pellets**
 - Squeezing fingers

- **Use of hot oil bath**
 - Burns

- **Use of acid and organic solutions**

- Spills on skin

Oversikt over besluttede risikoreduserende tiltak med beskrivelse:

Use of high temperature furnace (farekilde)

Use of high temperature furnace/Electric shock (uønsket hendelse)

Samlet sannsynlighet vurdert for Lite sannsynlig (2)
hendelsen:

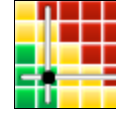
Kommentar til vurdering av sannsynlighet:

[Ingen registreringer]

Vurdering av risiko for følgende konsekvensområde:

Helse

Vurdert sannsynlighet (felles for hendelsen): Lite sannsynlig (2)



Vurdert konsekvens: Middels (2)

Kommentar til vurdering av konsekvens:

[Ingen registreringer]

Use of high temperature furnace/Uncontrolled heating (uønsket hendelse)

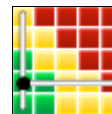
Samlet sannsynlighet vurdert for hendelsen: Lite sannsynlig (2)

Kommentar til vurdering av sannsynlighet:

[Ingen registreringer]

Vurdering av risiko for følgende konsekvensområde: Helse

Vurdert sannsynlighet (felles for hendelsen): Lite sannsynlig (2)



Vurdert konsekvens: Liten (1)

Kommentar til vurdering av konsekvens:

[Ingen registreringer]

Use of high temperature furnace/Fire (uønsket hendelse)

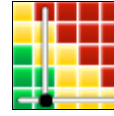
Samlet sannsynlighet vurdert for hendelsen: Svært lite sannsynlig (1)

Kommentar til vurdering av sannsynlighet:

[Ingen registreringer]

Vurdering av risiko for følgende konsekvensområde: Helse

Vurdert sannsynlighet (felles for hendelsen): Svært lite sannsynlig (1)



Vurdert konsekvens: Middels (2)

Kommentar til vurdering av konsekvens:

[Ingen registreringer]

Use of high temperature furnace/Burn damage (uønsket hendelse)

Samlet sannsynlighet vurdert for hendelsen: Lite sannsynlig (2)

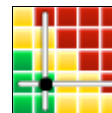
Kommentar til vurdering av sannsynlighet:

[Ingen registreringer]

Vurdering av risiko for følgende konsekvensområde:

Helse

Vurdert sannsynlighet (felles for hendelsen): Lite sannsynlig (2)



Vurdert konsekvens: Middels (2)

Kommentar til vurdering av konsekvens:

[Ingen registreringer]

Use of compressed gases (farekilde)

Use of compressed gases/Uncontrolled expansion and depletion of O₂ (uønsket hendelse)

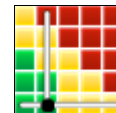
Samlet sannsynlighet vurdert for hendelsen: Svært lite sannsynlig (1)

Kommentar til vurdering av sannsynlighet:

[Ingen registreringer]

**Vurdering av risiko for følgende konsekvensområde:
Helse**

Vurdert sannsynlighet (felles for hendelsen): Svært lite sannsynlig (1)



Vurdert konsekvens: Middels (2)

Kommentar til vurdering av konsekvens:

[Ingen registreringer]

Use of compressed gases/Gas leakage (uønsket hendelse)

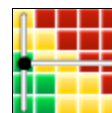
Samlet sannsynlighet vurdert for hendelsen: Sannsynlig (3)

Kommentar til vurdering av sannsynlighet:

[Ingen registreringer]

**Vurdering av risiko for følgende konsekvensområde:
Helse**

Vurdert sannsynlighet (felles for hendelsen): Sannsynlig (3)



Vurdert konsekvens: Liten (1)

Kommentar til vurdering av konsekvens:

[Ingen registreringer]

Use of chemicals as precursors (farekilde)**Use of chemicals as precursors/Spills on skin (uønsket hendelse)**

Samlet sannsynlighet vurdert for hendelsen: Sannsynlig (3)

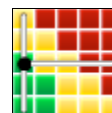
Kommentar til vurdering av sannsynlighet:

[Ingen registreringer]

**Vurdering av risiko for følgende konsekvensområde:
Helse**

Vurdert sannsynlighet (felles for hendelsen): Sannsynlig (3)

Vurdert konsekvens: Liten (1)



Kommentar til vurdering av

konsekvens:

[Ingen registreringer]

Preparation of pellets (farekilde)

Preparation of pellets/Squeezing fingers (uønsket hendelse)

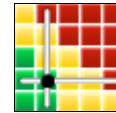
Samlet sannsynlighet vurdert for Lite sannsynlig (2)
hendelsen:

Kommentar til vurdering av sannsynlighet:

[Ingen registreringer]

Vurdering av risiko for følgende konsekvensområde:**Helse**

Vurdert sannsynlighet (felles for hendelsen): Lite sannsynlig (2)



Vurdert konsekvens: Middels (2)

Kommentar til vurdering av konsekvens:

[Ingen registreringer]

Use of hot oil bath (farekilde)

Use of hot oil bath/Burns (uønsket hendelse)

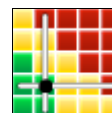
Samlet sannsynlighet vurdert for Lite sannsynlig (2)
hendelsen:

Kommentar til vurdering av sannsynlighet:

[Ingen registreringer]

Vurdering av risiko for følgende konsekvensområde: Helse

Vurdert sannsynlighet (felles for Lite sannsynlig (2)
hendelsen):



Vurdert konsekvens: Middels (2)

Kommentar til vurdering av
konsekvens:

[Ingen registreringer]

Use of acid and organic solutions (farekilde)**Use of acid and organic solutions/Spills on skin (uønsket hendelse)**

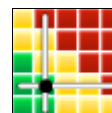
Samlet sannsynlighet vurdert for Lite sannsynlig (2)
hendelsen:

Kommentar til vurdering av sannsynlighet:

[Ingen registreringer]

**Vurdering av risiko for følgende konsekvensområde:
Helse**

Vurdert sannsynlighet (felles for Lite sannsynlig (2)
hendelsen):



Vurdert konsekvens: Middels (2)

Kommentar til vurdering av
konsekvens:

[Ingen registreringer]

Oversikt over besluttede risikoreduserende tiltak:

Under presenteres en oversikt over risikoreduserende tiltak som skal bidra til å reduseres sannsynlighet og/eller konsekvens for uønskede hendelser.

Oversikt over besluttede risikoreduserende tiltak med beskrivelse: